Divergence of excited state Møller–Plesset series: A complex issue

Diana-Gabriela Oprea

Christ Church

A thesis submitted for the Honour School of Chemistry

Part II 2022

Acknowledgements

First of all, I would like to thank my supervisor, Dr Hugh Burton, for his amazing insight into electronic structure theory, and for always being a source of new ideas which have led to the productive conversations shaping this project. I also want to thank him for all the advice, guidance and encouragement that I so much needed at times. Thank you to everyone in the Tew group for all the great meetings, presentations and discussions that allowed me to understand and explore electronic structure theory well beyond my project.

Thank you to my friends and family for supporting me in ways I did not always know I needed during this year and throughout my degree.

Summary

Excited states in molecules can be difficult to investigate. The methods that are generally used are either computationally expensive or not accurate enough. Simpler methods, such as MP2, are believed not to be suitable for excited systems because of the rich structure of near-degeneracies and because of the reliability on the Hartree-Fock algorithm, which is not designed to converge on excited states.

This work presents a systematic analysis of the application of single-reference perturbation theory to closed-shell excited states. Compared here are methods both for treating excited states at the Hartree-Fock level and different ways of approaching the issue of near-degeneracies that cause divergences in the perturbation expansions of the systems analysed, such as the imaginary level shift or extrapolation using quadratic approximants. Complex analysis is used to explore the singularities of these systems in order to understand the underlying mathematical structure that is responsible for the divergences observed. This treatment is applied to small molecules and atoms, namely H_2, Be, HF, and H_2O.

Contents

List of Figures

List of Abbreviations

CASPT2 . . . Complete active space second order perturbation theory

CC . . . . . Coupled-cluster

CI . . . . . Configuration interaction

EP . . . . . Exceptional point

FCI . . . . . Full configuration interaction

HF . . . . . Hartree-Fock

MO . . . . . Molecular orbital

MOM . . . . . Maximum overlap method

MP . . . . . Møller–Plesset

MP2 . . . . . Second order Møller–Plesset perturbation theory

NOCI . . . . . Non-orthogonal configuration interaction

SCF . . . . . Self-consistent field

1 Introduction

The field of theoretical and computational chemistry aims to predict and explain the chemical and physical properties of any chemical system, solely relying on the mathematical theory of electrons in atoms and molecules. While most of the research focuses on determining such properties in the ground state of a system, there is increasing interest in the investigation of excited states, which play a crucial role in the field of photophysics and photochemistry.[1]

The mathematical description of electrons and molecules is given by Ψ, the wave function, which contains all the information about a system. The wave function can be given a probabilistic interpretation, so that it can be used to determine the probability of measuring any physical observable.[2] The wave function is the solution to the Schrödinger equation:

$$\hat{H}_k \Psi_k = E_k \Psi_k, \tag{1.1}$$

where $\hat{H}$ is the Hamiltonian operator and E_k is the energy of the system in state Ψ_k. The Schrödinger equation has multiple solutions, which represent the ground and excited state wave functions, each of them corresponding to a different E_k.

However, solving the Schrödinger equation is extremely difficult and only systems that contain a maximum of two electron can be solved analitically. Therefore, it is necessary to develop models and approximate methods for describing the electronic structure of more complex systems.

The simplest and most widely used method is based on the Hartree-Fock (HF) theory.[3] The HF method is a mean field approach, in which the wave function is expressed as an anti-symmetrised product of single-electron wave functions, the molecular orbitals.

During a HF calculation, the energy is minimised with respect to the set of molecular orbitals used to build the wave function. The global minimum corresponds to the ground state of the system. However, the calculation can converge on higher-energy solutions which are local minima and correspond to HF excited states.[4,5,6]

Because it is a mean-field method, HF theory does not account for electron correlation, which causes it to fail at describing electronic structure at a quantitative level, and sometimes even at a qualitative one.

A common approach to overcome this issue in HF theory is to use the solutions from HF calculations and to build the electron correlation on top of them. Such methods include Møller-Plesset (MP) perturbation theory,[7] and coupled-cluster (CC) theory.[8,9]

The simplest and least computationally expensive correlation method is perturbation theory, in particular MP2, which uses the Møller-Plesset expansion up to the second order, and usually gives reasonable results for ground state energies.[10] Nevertheless, for this method to be systematically improvable, the series needs to converge, but the cost of computing higher-order terms is too high so convergence is not usually checked when performing an MP2 calculation.

Perturbation theory has generally been avoided in excited state calculations,

because degeneracies and near-degeneracies are known to cause divergences in the perturbation series. Nevertheless, recently there has been growing interest in using higher-energy HF solutions as approximations for excited states.[4,5] Given the difference in cost between MP2 and other methods, it is worth assessing the extent to which a single-configuration perturbative approach can be used for electronic structure theory, whether it fails or not, the exact cause of the failure, and the possible solutions that can make MP2 a more useful method in an excited state context.

This thesis focuses on the description of excited states using perturbation theory. In Chapter 2 the HF and MP approaches are described in more detail and the methodology and computational details are given. Chapter 3 shows the results for the H_2 molecule, while Chapter 4 explores some more complex systems (Be, HF, H_2O).

2
Theoretical Methods

Contents

All the information about a system is contained in its wave function, Ψ, which is the solution of the Schrödinger equation:[11]

$$\hat{H}\Psi = E\Psi, \tag{2.1}$$

where $\hat{H}$ is the Hamiltonian of the system and E is the energy. In the case of an atom or molecule,

$$\hat{H} = -\sum_{A=1}^{N} \frac{1}{2m_A}\nabla_A^2 - \sum_{i=1}^{n} \frac{1}{2}\nabla_i^2 + \sum_{A<B}^{N} \frac{Z_A Z_B}{R_{AB}} - \sum_{i=1}^{n}\sum_{A=1}^{N} \frac{Z_A}{r_{iA}} + \sum_{i<j}^{n} \frac{1}{r_{ij}}, \tag{2.2}$$

where N, n are the numbers of nuclei and electrons, respectively, m_A, Z_A are the mass and charge of nucleus A, R_{AB} is the distance between nuclei A and

B, r_{iA} is the distance between electron i and nucleus A, and r_{ij} is the distance between electrons i and j. Because electrons are much smaller than the nuclei and therefore move much more rapidly, it can be assumed that the electron cloud adapts instantaneously to any movement of the nuclei. Therefore, the movement of the nuclei and electrons can be decoupled, allowing the Hamiltonian to be written as the sum of a nuclear and an electronic Hamiltonian:

$$\hat{H} = \hat{H}_n + \hat{H}_e \tag{2.3}$$

Equation 2.3 implies that the wave function is also separable in a nuclear and electronic part, which is known as the Born-Oppenheimer approximation.[12] This allows the calculation of the electronic wave function for different positions of the nuclei, assuming those positions are fixed. In this work, we will focus on that, namely the electronic part of the Schrödinger equation:

$$\hat{H}_e \Psi_e = E_e \Psi_e \tag{2.4}$$

A second common approximation is the orbital approximation, which places each electron in a single-electron wave function, the so-called 'orbital'.[11] Molecular orbitals are usually expressed in terms of the atomic orbitals. This is done by using a finite set of basis functions. Usually, each basis function represents a single-electron atomic orbital.

The use of a finite basis set is also an approximation which allows the full Hamiltonian in the finite basis to be constructed and diagonalised, which is equivalent to solving the Schrödinger equation in the finite basis set and is known in literature as the full configuration interaction (FCI) method.[3] The eigenvalues are the exact energies of the ground and excited states of the system in the basis set. However, this method scales factorially with the size of the system so it can only be used for the smallest of systems.

The difficulty in solving equation 2.4 for any system with more than two electrons makes the determination of the electronic structure of different systems (discrete molecules, networks etc.) the bottleneck in most theoretical studies. Therefore, a series of approximate methods needs to be developed.

2.1 Hartree-Fock Theory

2.1.1 Theory

Hartree-Fock (HF) theory is a mean field approach to electronic structure theory.[3] For any system, the HF wavefunction is a single Slater determinant of the form:

$$\Phi = \hat{\mathcal{A}} \prod_{i=1}^{n} \phi_i \tag{2.5}$$

where $\hat{\mathcal{A}}$ is the anti-symmetriser,[11] which ensures that the wave function obeys the Pauli exclusion principle, and ϕ are the molecular orbitals in the chosen basis set. The HF energy is defined as:

$$E_{HF} = \frac{\langle \Phi | \hat{H} | \Phi \rangle}{\langle \Phi | \Phi \rangle} = V_N + \sum_{i}^{N} h_{ii} + \sum_{i}^{N} \sum_{j<i}^{N} \langle ij||ij \rangle \tag{2.6}$$

where N is the number of electrons in the system, V_N is the interaction between the fixed nuclei, h_{ii} are the diagonal matrix elements of the one-electron part of equation 2.2 and $\langle ij||ij \rangle$ is the simplified notation for the anti-symmetrised two-electron integrals:

$$\langle ij||ij \rangle = \langle \Phi_i \Phi_j | r_{12}^{-1} | \Phi_i \Phi_j \rangle - \langle \Phi_i \Phi_j | r_{12}^{-1} | \Phi_j \Phi_i \rangle \tag{2.7}$$

The optimal energy is found using the variational principle, by minimising the energy with respect to the molecular orbitals that are used to construct the Slater determinant.[3] This leads to a set of secular equations known as the Hartree-Fock equations:

$$\hat{F}_i \phi_i = \epsilon_i \phi_i \tag{2.8}$$

where $\hat{F}$ is the single-particle Fock operator:

$$\hat{F} = \hat{h} + \sum_k (\hat{J}_k - \hat{K}_k), \tag{2.9}$$

where $\hat{h}$ represents the one-electron terms in equation 2.2, and $\hat{J}_k$, $\hat{K}_k$ are the Coulomb and exchange operators, respectively, for each of the electrons in the system. The matrix elements of the Fock operator are:

$$F_{ij} = h_{ij} + \sum_k \langle ik||jk\rangle \tag{2.10}$$

Therefore, the Fock operator depends on the optimal orbitals that we need to solve for in the set of equations 2.8, so the HF is a self-consistent method, which involves the following steps:

1. Provide an initial guess of the orbitals;
2. Construct the Fock matrix using the initial guess;
3. Solve the HF equations using the Fock operator;
4. Construct a new Fock matrix using the solutions from the previous step;
5. Repeat until convergence is reached (i.e. the energy in two consecutive iterations does not change within a certain margin.)

2.1.2 Multiple HF Solutions and Excited States

The solutions of the HF method can be made to respect all the symmetries of the system, and this gives the restricted HF (RHF) solution. It is found that this solution does not always correspond to the minimum in the energy and the RHF approach cannot accurately describe all the systems e.g. it fails to describe the homolytic dissociation of a H_2 molecule. If the α and β electrons are allowed to occupy different spin-orbitals, the unrestricted HF (UHF) solution is found, which

is no longer an eigenfunction of the spin-operator, $\mathcal{S}$. The UHF state predicts the correct energy for the homolytic dissociation of H_2 by correctly localising one electron on each atom site. This solution only appears for the stretched H_2 molecule and does not exist at all geometries. The appearance of additional HF solutions is not unique to this system, but appears in a range of molecules.[13,14]

The existence of multiple HF solutions represents a point of interest for us, as they can be interpreted as mean-field excited states.

In this work, we are going to use two methods for constructing the reference Hamiltonian:

- **Δ-SCF**.[5] In this method, the self-consistent field calculation is done for the ground state. After obtaining the solution for the ground state, higher energy orbitals, corresponding to the targeted excited state, are populated. This method is equivalent to considering that the orbitals of ground states and excited states are the same;

- **MOM-SCF**.[4] It is actually known that ground state and excited state orbitals are different, sometimes to a great degree, so a better way of handling excited states should be by using the optimal orbitals. In order to find these, we are using the maximum overlap method (MOM), which accounts for orbital relaxation upon excitation of electrons. MOM-SCF is similar to normal Hartree-Fock, but the condition of choosing a new set of orbitals is changed. In HF, the new orbitals are always chosen so as to minimise energy and they are occupied following the aufbau protocol, whereas in MOM-SCF the condition of choosing a new set of orbitals is the maximum overlap with the previous set of orbitals. In order for this to work, the MOM-SCF procedure needs to have an initial guess that is close to the target excited state. Therefore, we

are using the excited states computed using Δ-SCF as the initial guess. The states using this method are true HF states, unlike the Δ-SCF states which are not stationary points on the energy landscape built using the ground state orbitals.

2.2 Møller–Plesset Perturbation Theory

The Møller-Plesset perturbation theory[7] is an example of the Rayleigh–Schrödinger perturbation theory.[15,16] In this latter method, a more complex problem is solved by expressing the Hamiltonian of the system as a sum between an unperturbed Hamiltonian, usually with known solutions or that can be computed, and a perturbation term, which is assumed to be small in comparison to the other term:

$$\hat{H} = \hat{H}_0 + \lambda \hat{H}_1 \tag{2.11}$$

where $\hat{H}_0$ is the unperturbed Hamiltonian, $\hat{H}_1$ is the perturbation and λ is a parameter used to keep track of the order of the correction and is usually set to 1 at the end of the computation. This allows us to get the energy as a function of λ, $E(\lambda)$, where $E(0)$ is the reference energy and $E(1)$ is the exact energy. λ can also be seen as a parameter controlling the extent of the perturbation, as for $\lambda = 0$ we have the unperturbed case and for $\lambda = 1$ we have the physical system. Intermediary values of λ allow only a fraction of the perturbation to be introduced into the system to be solved.

The underlying assumption is that the perturbation is small so that the solutions of the perturbed system are similar to the unperturbed states. The eigenvalues and eigenstates can then be approximated as power series of the parameter λ:

$$E_n = \sum_{i=0}^{\infty} E_n^{(i)} \lambda^i \tag{2.12}$$

$$\Psi_n = \sum_{i=0}^{\infty} \Phi_n^{(i)} \lambda^i \tag{2.13}$$

where $E_n^{(i)}$ and $\Phi_n^{(i)}$ are the i^{th} order corrections to the n^{th} energy and state, respectively.

The terms of the two series are found by introducing equations 2.11, 2.12, 2.13 into the Schrödinger equation and equating terms with the same power of λ, up to any desired order. For example, the expression for the second order correction,[11] which is most widely used in practice, is:

$$E_n^{(2)} = \langle \Phi_n^{(0)} | \hat{H}_1 (\hat{H}_0 - E_0)^{-1} \hat{H}_1 | \Phi_n^{(0)} \rangle \tag{2.14}$$

For diagonal unperturbed Hamiltonians, which is the case for all calculations in this thesis, equation 2.14 translates to:

$$E_n^{(2)} = \sum_{k \neq n} \frac{| \langle \Phi_k^{(0)} | \hat{H}_1 | \Phi_n^{(0)} \rangle |^2}{E_n^{(0)} - E_k^{(0)}} \tag{2.15}$$

Most calculations stop at MP2 level, which usually gives reasonable results and is computationally cheap. Higher-order of the perturbation series are more expensive and the accuracy does not justify the cost. However, in order to study the convergence of the series, we need to be able to find higher-order terms. The following general formulae can be easily derived using the same method:[3]

$$E_n^{(k)} = \langle \Phi_n^{(0)} | \hat{H}_1 | \Phi_n^{(k-1)} \rangle \tag{2.16}$$

$$\Phi_n^{(k)} = \left(\hat{H}_0 - E_n^{(0)} \right)^{-1} \left(\sum_{i=1}^{k} E_n^{(i)} \Phi_n^{(k-1)} - \hat{H}_1 \Phi_n^{(k-1)} \right) \tag{2.17}$$

Once λ is set to 1, the physical solution of the system is obtained.

For Møller-Plesset theory, the zeroth-order wavefunction is the Slater determinant introduced in equation 2.5, and the unperturbed Hamiltonian is given by the sum of the one-particle Fock operators:

$$\hat{H}_0 = \sum_i \hat{F}_i, \tag{2.18}$$

The perturbation is the difference between the full Hamiltonian and the unperturbed one:

$$\hat{H}_1 = \hat{H} - \hat{H}_0 \tag{2.19}$$

and

$$\hat{H} = \hat{H}_0 + \lambda(\hat{H} - \hat{H}_0) \tag{2.20}$$

The full Hamiltonian and the unperturbed Hamiltonian have been computed using the Slater-Condon rules (See Appendix A).

The Møller-Plesset theory is the most natural formulation of a perturbation series for electronic structure, because it starts with a Hartree-Fock calculation, the most common mean-field method. Nevertheless, MP is found to fail in many cases, especially for strongly correlated or near-degenerate states, as the single-reference approach taken is not suitable for these systems.[10,17,18]

2.3 Convergence

The Møller–Plesset series obtained using the method described in the previous section can be truncated at any term, giving MP2, MP3, MP4 etc. It is useful to note that the MP1 energy is just the Hartree-Fock energy:[11]

$$E^{(0)} + E^{(1)} = E_{HF} \tag{2.21}$$

The most commonly used method is MP2, because it is found to give reasonable energies, while being relatively cheap, scaling as $\mathcal{O}(N^5)$.[10] In principle, the MP series should converge to the exact result for $n \to \infty$. However, in many instances it is known that the series is actually divergent or converges slowly even for systems that are considered to be well understood,[19,20] meaning that the approximation gets increasingly worse for larger n. Nevertheless, the convergence of the MP series

is not checked when performing MP2 calculations, as it gets increasingly expensive to compute higher-order terms. Therefore, while the MP2 gives accurate results in some cases, the reliability of low-order approximations is called into question.

Radius of convergence. The values of λ that give a convergent series are defined by the radius of convergence of that series. The radius of convergence is, mathematically speaking, the radius of the largest disc inside which the series converges.[21]

In more applied terms, the radius of convergence for a function is equal to the distance from the origin of the closest singularity in the complex plane.[22] A singularity or a singular point of a complex variable is a point at which the function is non-analytic (it cannot be expressed as an infinite power series). Singularities can be classified in categories, of which of particular interest to this work are branch points and poles.[21]

For functions that diverge, the radius of convergence is equal to 0, while for series that converge for some values of the λ, it has a finite non-negative value. One way of calculating it is the following limit:[23]

$$\frac{1}{r_c} = \lim_{k\to\infty} \frac{E_{k+1}}{E_k} \tag{2.22}$$

Another way, more geometrical, to compute the radius of convergence is related to the singularity structure of the function *E(λ)* is to find the distance of the singularity that is closest to the origin.[21] This singularity is referred to as the dominant singularity.

$$r_c = |\lambda_{DS}| \tag{2.23}$$

The case of interest for us is the physical problem, for which $\lambda = 1$. It is then necessary for the radius of convergence to be greater than 1, therefore that the

dominant singularity is found outside of the unit circle.

2.3.1 Exceptional points

Exceptional points (EPs) are square-root branch points, a type of singularity that is particularly common in electronic structure. They arise from the non-Hermitian Hamiltonian which results from extending equation 2.11 to complex λ values.[24] At an EP, two states become degenerate and identical - they are known as self-orthogonal states.[25]

This can be more easily understood by means of a two-level model, for which the Hamiltonian is written as:

$$H = \underbrace{\begin{pmatrix} \epsilon & 0 \\ 0 & -\epsilon \end{pmatrix}}_{H_0} + \lambda \underbrace{\begin{pmatrix} 0 & \delta \\ \delta & 0 \end{pmatrix}}_{H_1} \tag{2.24}$$

This Hamiltonian can be diagonalised to give the exact energy levels:

$$E(\lambda) = \pm\sqrt{\epsilon^2 + \lambda^2\delta^2} \tag{2.25}$$

The two solutions become degenerate when the expression under the square root is 0. The points at which this happens are exceptional points at $\lambda = \pm\frac{i\epsilon}{\delta}$ and are related to the radius of convergence of the perturbation series of the same system:

$$r_c = |\lambda_{EP}| = \left|\frac{\epsilon}{\delta}\right| \tag{2.26}$$

For each value of $\frac{\epsilon}{\delta}$, there are two exceptional points found at complex conjugate values of λ. Therefore, for $\left|\frac{\epsilon}{\delta}\right| > 1$, the perturbation series is convergent, while for $\left|\frac{\epsilon}{\delta}\right| < 1$, it is divergent. This agrees with our intuition, as the perturbation series is expected to fail if the perturbation Hamiltonian is comparable in magnitude to the unperturbed Hamiltonian. This is illustrated in Figure 2.1. Figures 2.1a and 2.1c show the Riemann surfaces[26] constructed by allowing λ to take complex values

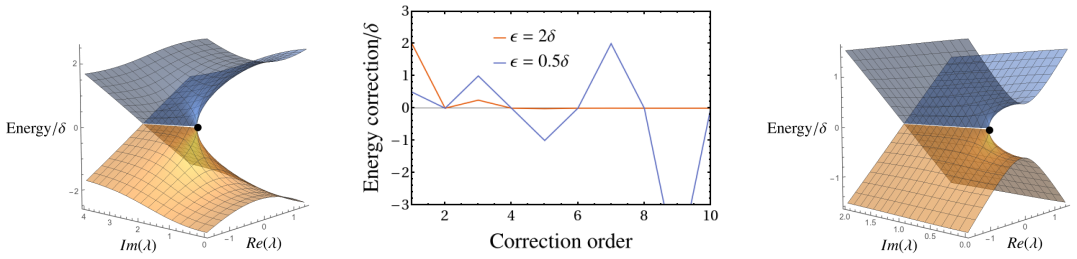

(a) $\epsilon = 2\delta$ **(b)** Perturbation series. **(c)** $\epsilon = 0.5\delta$

Figure 2.1: Exceptional points (given by the black dots) in the two-level model at different values of ϵ/δ and the correlation between the position of the EP and the convergence or divergence of the perturbation series at $\lambda = 1$.

in the expression from equation 2.25. A Riemann surface is a one-dimensional complex manifold.[27] In this case, each sheet corresponds to a different solution. In the case of Figure 2.1a, the EPs are found at $\pm 2i$ (only one of them shown for clarity) and the perturbation series is convergent for $\lambda = 1$, while in Figure 2.1c, the EPs are found at $\pm 0.5i$ and the series is divergent.

The states that become degenerate with the reference or target state causing divergences in the perturbation series are called *intruder states* in the literature.[28] Depending on whether they are found on the negative real axis or on the positive real axis, they are referred to as *back-door intruders* and, respectively, *front-door intruders*.[29]

The physical interpretation of the intruder states has been investigated in other works.[18,29,30,31,32] They are sometimes low-lying excited states, but they have also been identified as highly excited states, such as one-electron ionisations. The concept of critical point has been introduced by Sergeev et al.[31] This is a singularity that appears on or close to the negative real axis and corresponds to the value of $\lambda < 0$ at which the interelectronic interaction (which is now attractive since λ is negative) overcomes the nuclear attraction and the electrons dissociate as a cluster.

Therefore, exceptional points connect states that are non-degenerate on the

real axis, but become degenerate in the complex plane. In the complex λ-space, the energy surfaces of different eigenstates that are discrete on the real axis are actually connected and form one Riemann surface with multiple sheets. This property allows for a continuous way of moving from one state to another by simply following a path in λ-space that encloses the EP.[33] By encircling the EP once, the state changes from the reference state to the intruder state state and only after a second loop does it go back to the reference state. This will be helpful in following chapters because it offers a relatively simple way of identifying the intruder states.

On the real λ-axis, the existence of an EP in the complex plane is manifested as an avoided crossing between the states that become degenerate. The position of the EP controls how sharp the avoided crossing is.[24] This can also be illustrated by the two-level model. There is a much sharper avoided crossing on the real axis in Figure 2.1c than in 2.1a. If the EP is far enough from the real axis, the avoided crossing is not observed, so the position of the exceptional point is indeed linked to the strength of the interaction between the coupling states.

2.3.2 Approximants

Locating the singularities of a system in order to assess whether a series converges or diverges is a preferred alternative to computing a large number of terms in the perturbation series. However, the exceptional points of the energy surfaces obtained by diagonalising the full Hamiltonian at different values of λ cannot be accurately found and characterised by a power series like the one produced by the MP perturbation theory, as there are no square-root branch points in it. Therefore, the singularity structure needs to be approached in a different way.

The way which has proven to be the most useful is that of using approximant methods, which consider a model function containing parameters that are chosen

so that its Taylor series agrees with the coefficients of the perturbation series up to some given order. If the functional form of the approximant is a good model of the true function, they will be able to reproduce the position of the EPs, as well as extrapolate the value of the function in cases where the MP series is divergent.

The two approximants we are going to use are the Padé linear and quadratic approximants,[21] which are useful for describing pole singularities and, respectively, square-root branch singularities.

The linear approximant is obtained by solving a equation of the form:

$$Q(\lambda)E(\lambda) - P(\lambda) = \mathcal{O}(\lambda^{n+1}) \tag{2.27}$$

where everything is defined in the same way as for the quadratic approximant and the coefficients can be found by solving a simpler system of linear equations. The linear approximants are written as $[n_1,\ n_2]$, where n_1 and n_2 are the orders of the two polynomials.

The energy can be approximated as:

$$E(\lambda) = \frac{P(\lambda)}{Q(\lambda)} \tag{2.28}$$

The poles can be found by setting the denominator in the expression 2.28 to 0. While we do not expect for the systems considered to have poles, the linear approximant is often found to give good approximation of the position of a singularity, even if it models it as the wrong type of singularity.

Similarly, the quadratic approximant is obtained by solving an equation of the form:

$$Q(\lambda)E^2(\lambda) + P(\lambda)E(\lambda) + R(\lambda) = \mathcal{O}(\lambda^{n+1}) \tag{2.29}$$

where n is the truncation order of the power series of $E(\lambda)$ and the polynomials

Q(λ), P(λ), R(λ) are defined as:

$$P(\lambda) = \sum_{k=1}^{d} p_k \lambda^k, Q(\lambda) = \sum_{k=1}^{d} q_k \lambda^k, R(\lambda) = \sum_{k=1}^{d} r_k \lambda^k \tag{2.30}$$

The order of these polynomials can be chosen and varied and the approximant is usually referred to as the $[n_1, n_2, n_3]$ quadratic approximant, where n_1, n_2, n_3 are the orders of the three polynomials. The coefficients p_k, q_k, r_k can be found by solving a system of linear equations and usually setting $q_0 = 1$. Therefore, the energy can be approximated as:

$$E(\lambda) = \frac{-P(\lambda) \pm \sqrt{P^2(\lambda) - 4Q(\lambda)R(\lambda)}}{2Q(\lambda)} \tag{2.31}$$

The branch points of the energy function are found by setting the polynomial under the square root to 0 and solving for λ. Depending on the order of the polynomials chosen, the number of roots may vary, so it is important to be able to find the roots that correspond to the genuine EPs.

While only the quadratic approximant is able to model the right type of singularity, both approximants give reliable estimations of the position of the singularities. Therefore, we can use both type of approximants to make sure the right positions of the EPs are found. As in both cases the positions of the singularities are determined by finding the roots of high order polynomials, there are usually multiple solutions, out of which some might have no significance, while others might be associated with non-dominant EPs.

In this work, we are going to simultaneously use different methods of determining the physical EPs and discarding the spurious roots:

- We compare the roots of the two types of approximants. Physical EPs are expected to be identified by both methods;

- We compute the approximants at different orders. Physical EPs are expected to be consistently found at all orders;
- For molecules, we can continuously change the geometry of the system. Physical EPs are expected to also change continuously, while spurious one will not show this behaviour.

We have found that the location of the EPs determined using the quadratic and linear approximants is a good indicator of the convergence or divergence of the corresponding series. However, depending on the order of the approximants being used, the perturbation series still needs to be computed up to at least 10 orders, which is significantly more expensive than the MP2.

2.4 Computational Details

The implementation of the methods described in the previous sections was done in `python3`. The `pyscf` package was used for HF calculations, including for the maximum overlap method, for which the `mom_occ()` built-in method was changed to also allow its use for RHF calculations. The HF calculations provides the molecular orbital energy and coefficients, as well as the atomic orbital integrals, which were used to compute the molecular orbitals integrals.

I wrote code to build the full and the reference Hamiltonians in the basis set chosen, using the Slater-Condon rules (See Appendix A). The expressions in equations 2.16 and 2.17 were implemented in order to compute the perturbation series up to any arbitrary order. I wrote code for both the RHF and UHF cases. For the latter, I also implemented the treatment of degenerate state via degenerate perturbation theory.

The calculation of approximants has been implemented by solving systems

of linear equations, as described in Ref. 34.

The energy landscapes used in Chapter 3 have been plotted in `Mathematica 12.0` using the method and code associated to Ref. 35.

The molecular diagrams in Chapter 4 and Appendix B were plotted using the `energydiagram` package that can be found at:
https://github.com/giacomomarchioro/PyEnergyDiagrams.

3
The Hydrogen Molecule

Contents

In order to illustrate the concepts introduced in this chapter, we investigate them in the context of the H_2 molecule. In particular, we look at the singularity structure in two different basis sets, STO-3G and 6-31G. In STO-3G, the H_2 molecule is very similar to the two-level model system used in the previous chapter.

3.1 Ground State

3.1.1 STO-3G

Working in a minimal basis set is very suited for illustrative purposes because the small dimension of the Hilbert space allows us to construct the Riemann surface

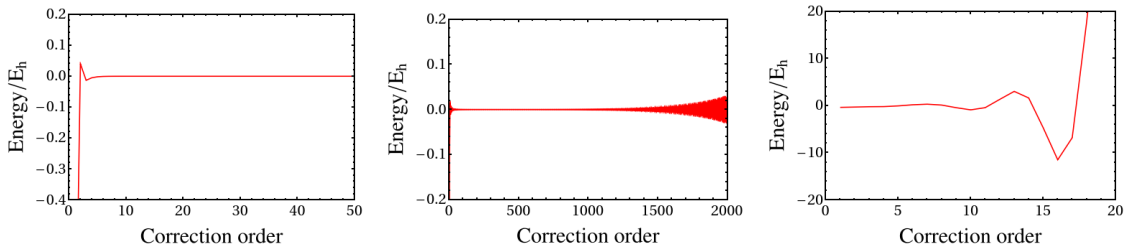

(a) Equilibrium, 0.74 Å **(b)** 2.06 Å **(c)** 3.00 Å

Figure 3.1: Ground state MP corrections for ground state H_2 at different bond lengths in STO-3G.

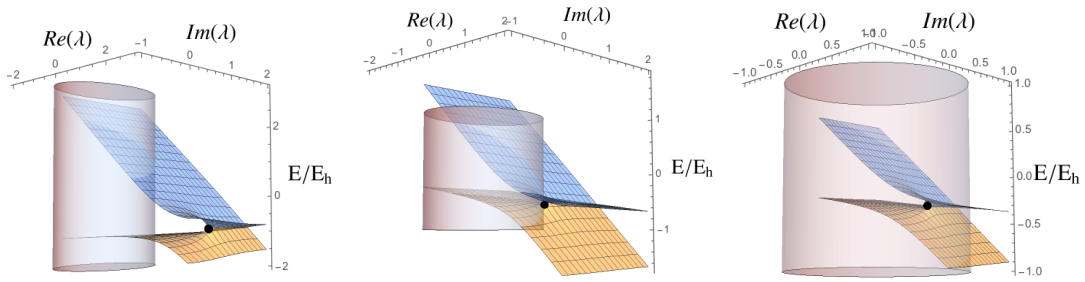

(a) 0.74 Å **(b)** 2.06 Å **(c)** 3.00 Å

Figure 3.2: Energy surfaces obtained by plotting the eigenvalues of the full Hamiltonian for complex values of λ, using the STO-3G basis set. The two surfaces shown correspond to the $1\sigma_g^2$ and $1\sigma_u^2$ states. The positions of the EPs are given by the black dots. In all cases, the cylinder has radius 1, showing how the exceptional points move inside it as the bond is stretched, causing divergence in the MP series.

and energy landscape of this system.

Figure 3.1 shows the energy corrections obtained using the MP theory at different bond lengths of the molecule. We found that at equilibrium, the series converges and, as the bond is stretched, it converges more and more slowly, until it finally diverges after 2.06 Å.

Figure 3.2 shows the energy surfaces obtained by diagonalising the full Hamiltonian for different values of λ. Only the closed-shell states are shown, as in this case there is no coupling between the closed-shell and the open-shell states. The surfaces corresponding to the $1\sigma_g^2$ and $1\sigma_u^2$ become degenerate at an EP that moves from outside the unit circle at equilibrium to inside the unit circle at long bonds. This behaviour of the EP mirrors the convergence pattern of the MP series.

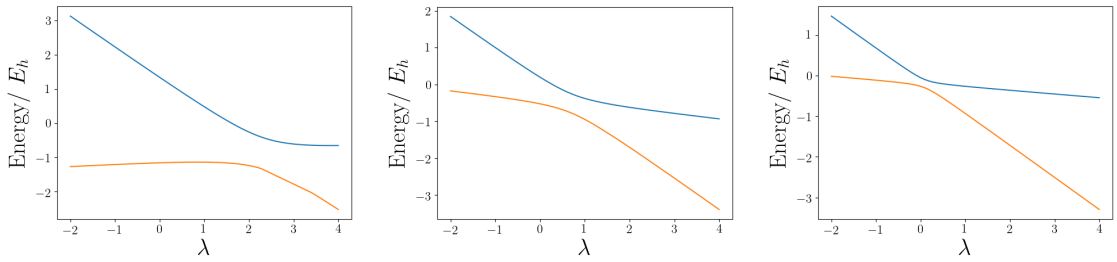

(a) 0.74 Å **(b)** 2.06 Å **(c)** 5.00 Å

Figure 3.3: Evolution of the avoided crossing between the $1\sigma_g^2$ and $1\sigma_u^2$ states at different bond lengths. As the bond is stretched, the crossing moves closer to the origin and becomes sharper.

This evolution can be understood in a more traditional way too, as an exceptional point gives raise to an avoided crossing on the real axis (Figure 3.3).[24] In particular, as the bond is stretched, the avoided crossing becomes sharper i.e. the two states become closer and closer in energy until they can be seen as quasi-degenerate. In the dissociation limit, the two reference states are fully degenerate, as the two electrons localise on one of the two atoms. As HF and MP perturbation theory rely on the approximation that the targeted state is in an area of the energy spectrum that is well-spaced, it is natural for them to fail upon bond stretching, when this condition is no longer satisfied. At even longer bond lengths, the avoided crossing becomes a cusp, which cannot be modelled by a polynomial.

The EP positions can be more precisely determined using the quadratic approximants introduced previously. The values computed using a [2, 2, 2] quadratic approximant are shown in Table 3.1 and confirm to a good degree the position of the exceptional points from Figure 3.2. In particular, at 2.06 Å, the EP is just slightly inside the unit circle, agreeing with the computed series which does diverge, but at a very slow rate.

It is also important to notice that if the EP is found on the unit circle or very close to it, as is the case for the 2.06 Å bond for H_2, the convergence of the

Bond length	EP	|EP|
0.74 Å	$2.35 \pm 0.926i$	2.53
2.06 Å	$0.688 \pm 0.719i$	0.995
3.00 Å	$0.292 \pm 0.493i$	0.552

Table 3.1: Exceptional points for H_2 in STO-3G, approximated with a [2,2,2] quadratic approximant.

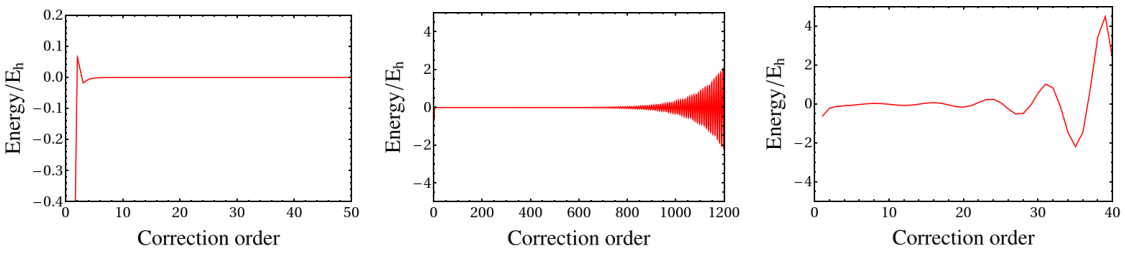

(a) 0.74 Å **(b)** 2.46 Å **(c)** 3.00 Å

Figure 3.4: MP corrections for ground state H_2 at different bond lengths in 6-31G.

series cannot be decided unless high-order terms are computed. In Figures 3.1a, 3.1c, the series is clearly converging and diverging from the first terms. However, in Figure 3.1b, the series seems to be converging for the first 500 terms, only to diverge later on. This is particularly worrying, as it means that the convergence of a series cannot be assessed just by looking at the first terms. It has been the case for systems that were considered well-understood and converging to find that the perturbation series actually diverges at higher order. In this thesis, we have found that the positions of the EPs computed using the approximants to be a reliable indicator of the convergence or divergence of the series. For this, only about 10 terms of the series are enough (depending on the order of the approximant used), which is significantly less than 500, but goes well beyond MP2.

Bond length	EP	|EP|
0.74 Å	$1.514 \pm 1.623i$	2.219
2.46 Å	$0.768 \pm 0.627i$	0.991
3.00 Å	$0.284 \pm 0.468i$	0.547

Table 3.2: Exceptional points for H_2 in STO-3G, approximated with a [2,2,2] quadratic approximant.

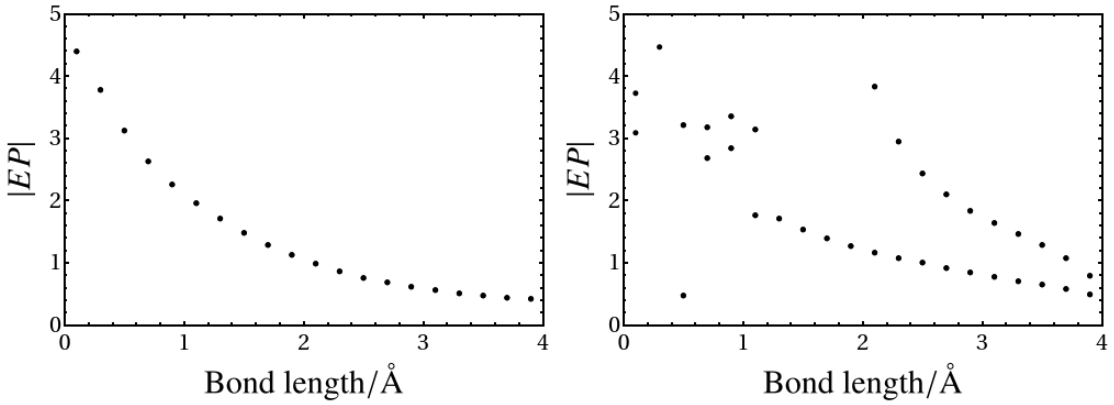

(a) STO-3G basis set. **(b)** 6-31G basis set.

Figure 3.5: Square-root branch points in the [2, 2, 2] quadratic approximant of the MP series of H_2 at different bond lengths.

3.1.2 6-31G

For larger basis sets or more complex systems, the direct inspection of the energy surfaces and the identification of EPs becomes difficult or impossible, while the approximants are still useful and give good estimates. Figure 3.4 shows the energy corrections of the MP series obtained for the ground state of H_2 at 0.74 Å, 2.46 Å, and 3.00 Å in 6-31G basis set, while Table 3.2 shows the position of the exceptional points for the same cases. The pattern is similar to that observed previously in STO-3G, but the divergence is observed at a longer bond, confirming that the convergence/divergence behaviour of the MP series depends on the basis set, as observed in previous work.[36,29]

The positions of the exceptional points tabulated in Tables 3.1 and 3.2 were selected from the roots of the quadratic approximant used to approximate the series. In order to make sure the right dominant singularities have been identified, we have made use of the observation that the EP seems to be getting gradually closer to the origin as the bond is stretched. Thus, by plotting the absolute values of the roots, it can be seen which of them show this evolution as the bond is stretched. This

is shown in Figure 3.5, where all roots with the absolute value below 5 have been plotted for the two cases considered. For STO-3G, there is only one root in the given interval and its absolute value changes continuously as the bond is stretched. The 6-31G picture is much more complex. There are two noticeable roots that evolve in a continuous manner as the bond is stretched. The lower one correspond to the dominant singularity, caused by the interaction between the $1\sigma_g^2$ and $1\sigma_u^2$ state, so it is the one mentioned in Table 3.2. The higher one corresponds to the interaction with a different state which is present in the larger Hilbert space of this system. There are also a number of spurious roots, especially at low bond lengths, but they are not preserved as the geometry is changed so they can be discarded.

3.2 Excited States

In the following, the perturbation series for the closed-shell excited state of H_2 in the two basis sets are investigated. We do this by using two different references for each excited state: the Δ-SCF[5] reference which is constructed by occupying higher-energy orbitals from the ground state, and the MOM-SCF[4] reference, which accounts for orbital relaxation in the excited state compared to the ground state.

3.2.1 STO-3G

In minimal basis set and using the Δ-SCF approach, the convergence behaviour of the MP series for the $1\sigma_u^2$ excited state mirrors that of the ground state discussed in the previous chapter, as it can be seen in figures 3.6a, 3.6b, 3.6c or in the MP2 and MP3 binding curves for the two states in figure 3.7a that diverge from the exact solution at the same bond length. This is because this method uses the same reference Hamiltonian for both the ground and excited state so the dominant EP is the same.

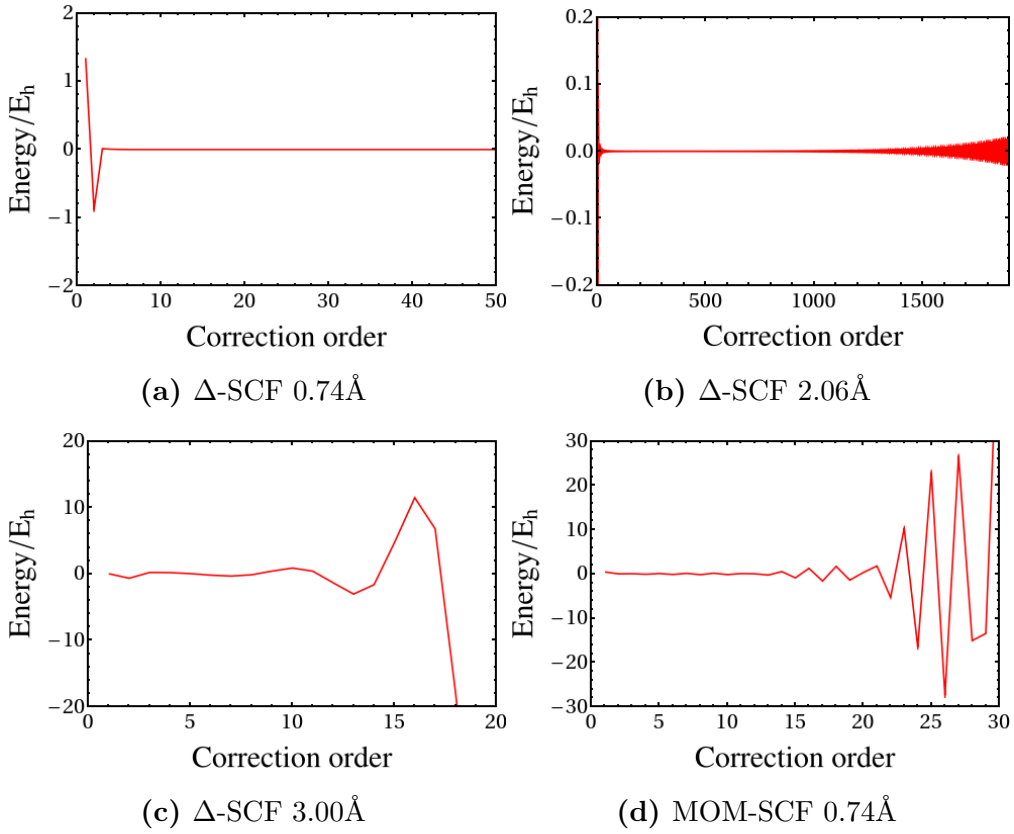

(a) Δ-SCF 0.74Å **(b)** Δ-SCF 2.06Å

(c) Δ-SCF 3.00Å **(d)** MOM-SCF 0.74Å

Figure 3.6: MP corrections for $1\sigma_u^2$ state H_2 at different bond lengths in STO-3G.

By allowing for orbital relaxation upon excitation, we find that the MP series for the $1\sigma_u^2$ excited state actually diverges even at equilibrium (figure 3.6d). The MP2 binding curve shown in figure 3.7b is a very poor approximation to the exact solution and a much poorer one than the one in figure 3.7a. The binding curve for the MOM-SCF MP2 has a discontinuity at 1.25Å, after which the perturbation series is clearly divergent. Therefore, not only does orbital optimisation not improve the accuracy of the perturbation series, but it actually gives worse results by causing the series to diverge.

3.2.2 6-31G

In a larger basis set, multiple excited states exist and the states responsible for the dominant EPs are less obvious. The binding curves for the closed-shell excited

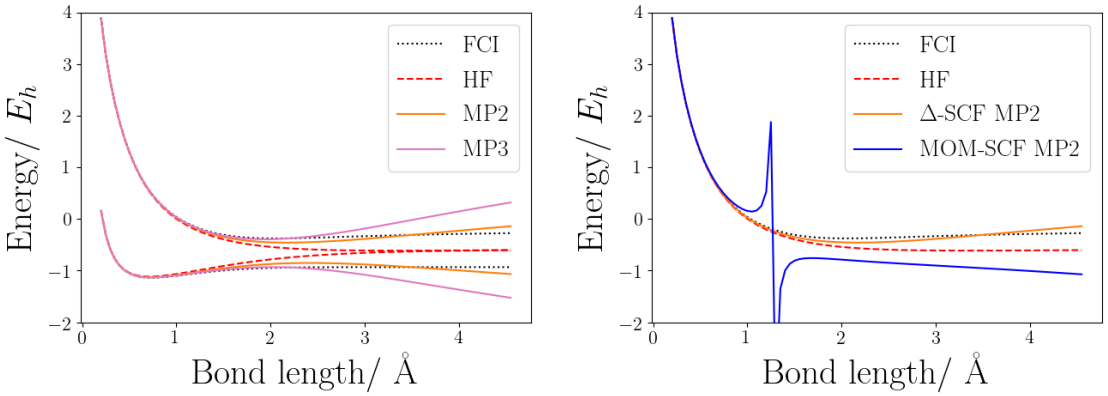

(a) Δ-SCF **(b)** MOM-SCF

Figure 3.7: Binding curves for H_2 in minimal basis set.

states in 6-31G basis set using the two methods are shown in figure 3.8.

The $1\sigma_g^2$ binding curves mirror those in STO-3G, with the Δ-SCF MP2 being a good approximation to the exact solution, while the MOM-SCF MP2 has a discontinuity and gives very poor results. The convergence behaviour is also similar, with the Δ-SCF perturbation series converging at shorter bonds and diverging at longer bonds. The series starts to diverge at a larger bond length, 2.46 Å, so the position of the exceptional point is dependent on the basis set. A larger basis set allows for more flexibility in the eigenstates so it is not a surprise that the series converges on a larger domain of bond lengths. On the other hand, the MOM-SCF perturbation series diverges at all bonds.

The $2\sigma_g^2$, $2\sigma_u^2$ states pose more difficulties because the unperturbed solutions become degenerate at two points in the 1-2Å interval, resulting in divergence at those points in the Δ-SCF. The series only converges up to 1 Å, but at points where it does not visibly diverge at MP2 level (0-1 Å and 2-3 Å), it is not a reasonable approximation of the exact solution. By applying MOM, the divergence caused by the degeneracy in the reference states is removed. However, the two series diverge at all bond lengths, while the binding curves have multiple discontinuities and

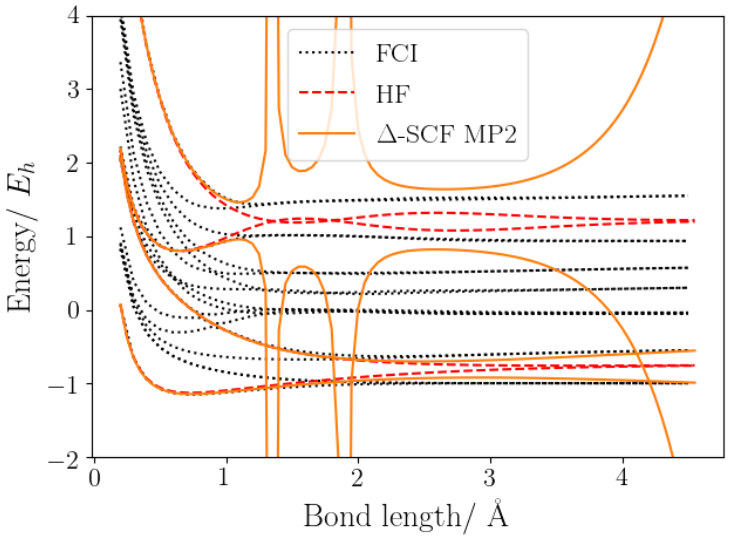

(a) Δ-SCF binding curves for $1\sigma_g^2$, $1\sigma_u^2$, $2\sigma_g^2$, $2\sigma_u^2$ states.

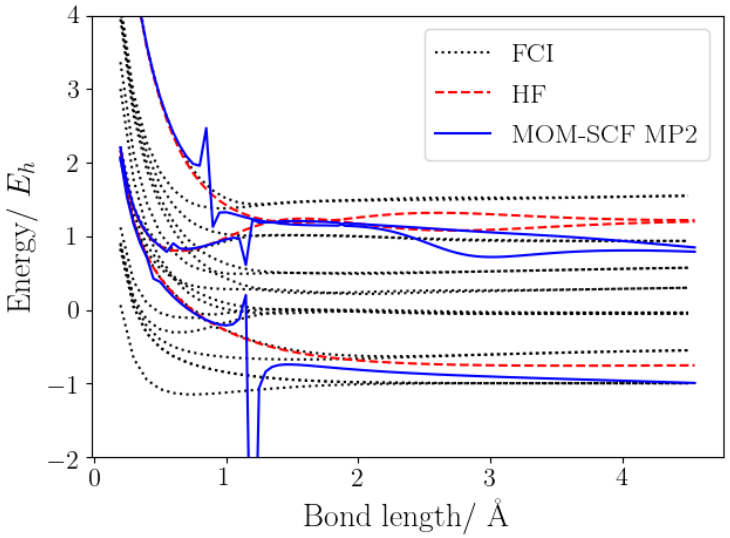

(b) MOM-SCF binding curves for $1\sigma_u^2$, $2\sigma_g^2$, $2\sigma_u^2$ states.

Figure 3.8: Binding curves in 6-31G basis set.

have poor accuracy.

3.2.3 Energy landscapes

In order to understand this unexpected result, we need to consider a different perspective: in short, a perturbation series is a Taylor-like expansion around a point on the reference energy landscape. This expansion gives better results the

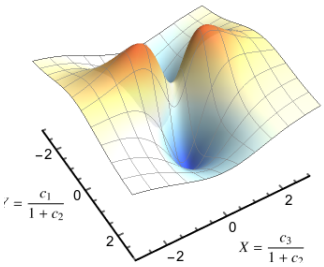

(a) Exact energy landscape at 0.74Å.

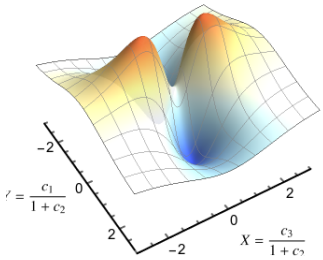

(b) Δ-SCF Fock energy landscape at for $1\sigma_u^2$ 0.74Å.

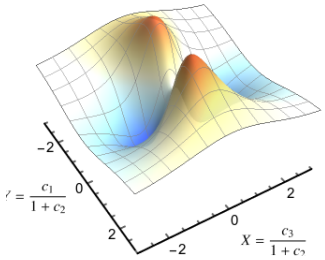

(c) MOM-SCF Fock energy landscape at $1\sigma_u^2$ 0.74Å.

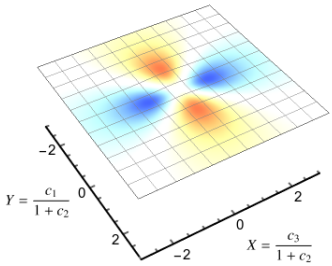

(d) Excited state Fock energy landscape at 1.25Å.

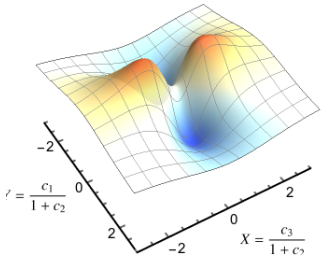

(e) Excited state Fock energy landscape at 2.5Å.

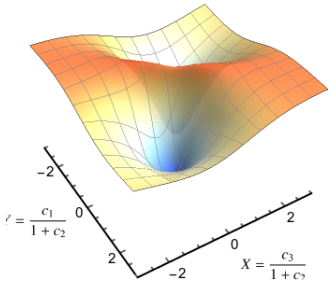

(f) Exact energy landscape at 2.5Å.

Figure 3.9: Energy landscapes for the H_2 molecule in the STO-3G basis.

better the reference energy landscape approximates the exact energy landscape. In order to visualise this, we construct the energy landscapes[35] by parametrising the singlet wave function for the system in minimal basis set as:

$$|\Psi(c_1, c_2, c_3)\rangle = c_1 \,|\bar{\sigma}_g \sigma_g\rangle + c_2(|\sigma_g \bar{\sigma}_u\rangle + |\bar{\sigma}_g \sigma_u\rangle) + c_3 \,|\bar{\sigma}_u \sigma_u\rangle \tag{3.1}$$

Two new coordinates are defined as:

$$X = \frac{c_3}{1 + c_2}, Y = \frac{c_1}{1 + c_2} \tag{3.2}$$

and the energy landscapes of different Hamiltonians constructed by plotting:

$$E(X, Y) = \langle \Psi(X, Y) | \hat{H} | \Psi(X, Y) \rangle \tag{3.3}$$

The resulting energy landscapes are plotted in figure 3.9. By inspecting the top row, which shows the landscapes for the exact Hamiltonian, the Δ-SCF, and

the MOM-SCF reference Hamiltonians for the $1\sigma_u^2$ state at equilibrium, it is easy to understand the difference between the two methods. The Δ-SCF landscape is qualitatively similar to the exact landscape, having the minima and maxima close to the exact positions and therefore the right sign of the gradients. On the other hand, in the MOM-SCF landscape, the minima and maxima are reversed so the expansion is built using the wrong first and second derivatives.

This also gives some insight into the effect of the MOM algorithm on the energy landscape: this procedure lowers the reference target state (in this case the $1\sigma_u^2$) in energy, turning it into a minimum. The discontinuity in the binding curve at 1.25 Å is also explained by the landscape, as this is the bond length at which the landscape is flat and the expansion changes from a negative gradient before 1.25 Å to a positive one after 1.25 Å. After this value, the targeted state becomes a maxima and the landscape is qualitatively similar to that in figure 3.9a, but the exact landscape does not have that shape (figures 3.9e and 3.9f). Therefore, the MOM-SCF landscape fails to approximate the exact one at all bond lengths, while the Δ-SCF is a good approximation at short bond lengths.

While these landscapes are constructed for the STO-3G basis set and similar landscapes are too complex to be analysed for larger basis sets, the previous two sections show that there is consistency in the results for the two cases, so we infer that the divergence in the MOM-SCF perturbation series for the larger basis set is explained by a similar change in the shape of the landscape.

3.3 Concluding Remarks

H_2 is a very simple molecule. However, the perturbative treatment of excited states for this system has proven to be quite difficult. The biggest challenge is that of degeneracies and near-degeneracies in the reference Hamiltonian. This issue was

not improved by using an optimised set of molecular orbitals, and it was found that for some states, orbital optimisation leads to an even more diverging series.

While the H_2 molecule provided some insight into the problem at hand, a two-electron system is quite restrictive. In order to check the general applicability of these conclusions, we proceed to some bigger, more complex systems.

4
Other Systems

Contents

In this chapter, we extend our research into excited states to bigger systems, yet small enough to allow the computation of the MP series up to high orders. We start by looking at Be, a small atom with a complex structure due to the many p-excited states. Then we return to the molecular realm with HF, another diatomic, and H_2O.

4.1 Be atom

The calculations for Be are done using the 6-31G basis set. The Hilbert space for this system has size 1296. While we are only going to focus on the closed-shell excited states, $1s^2 3s^2$ and $2s^2 3s^2$, we expect a rich interaction network with the large number of states. Figure 4.1 shows the evolution of the energies of the singlet

State	Method	MP2/E_h	MP3/E_h	FCI/E_h
$1s^2 3s^2$	Δ-SCF	-13.7320709	-13.8892314	-13.6579143
	MOM-SCF	-13.5894256	-13.6300386	-13.6579143
$2s^2 3s^2$	Δ-SCF	-3.61022795	-4.78939841	-3.4499377
	MOM-SCF	-3.4759369	-3.6787047	-3.4499377

Table 4.1: Be closed-shell excited state MP energies.

states as λ is varied on the real axis. By inspecting this figure, we expect MP perturbation theory to fail because of at least two reasons:

- the density of states is really high and the states come in "packets" in which all states are near-degenerate;
- there are visible avoided crossings on the real axis, which are signs of exceptional points close to the real axis.

The ground state perturbation series does converge and it can be seen in figure 4.1 that the ground state energy is found in an area with low density of states, therefore being shielded from the issue of near-degeneracy. On the other hand, the two closed-shell excited states energies are found in areas with high density of states, so it expected to have difficulties in computing the perturbation series for these states.

As predicted, the MP series for Be excited states diverges for both closed-shell excited states in both methods. The values for the MP2, MP3 and exact energies for these states are found in Table 4.1.

Constructing energy landscapes in order to visualise how good the reference states used are is too difficult in such a complex system. Nevertheless, we can still assess the quality of the reference wave function by checking whether it is an appropriate approximation of a single exact state or if it has significant contributions from more than one state. Any reference function can be written as a linear

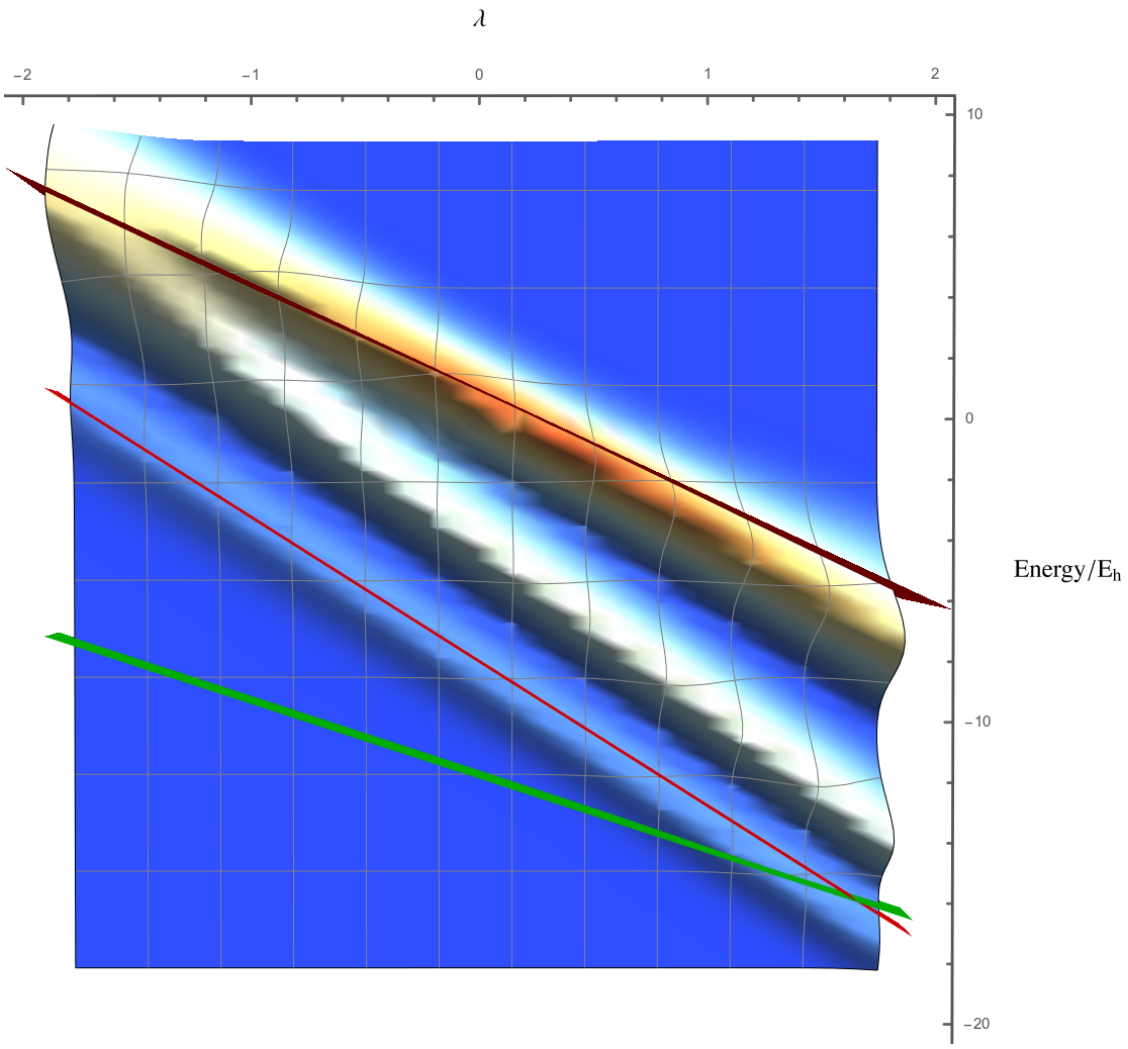

Figure 4.1: Density of states at different values of λ. The planes represent the energies of the reference state tracked in the λ-space. The green plane is the ground state, while the black planes are the $1s^2 3s^2$ and $2s^2 3s^2$ closed-shell excited states.

combination of the exact solutions:

$$\Phi = \sum_i c_i \Psi_i \tag{4.1}$$

This is the reverse of our normal intuition, in which the exact state is expressed as a linear combination of Slater determinants. However, this is just a change of basis, which can be performed in both directions.

A good reference function should have a high contribution from only one state so that there is a mapping between the exact and the unperturbed states. This

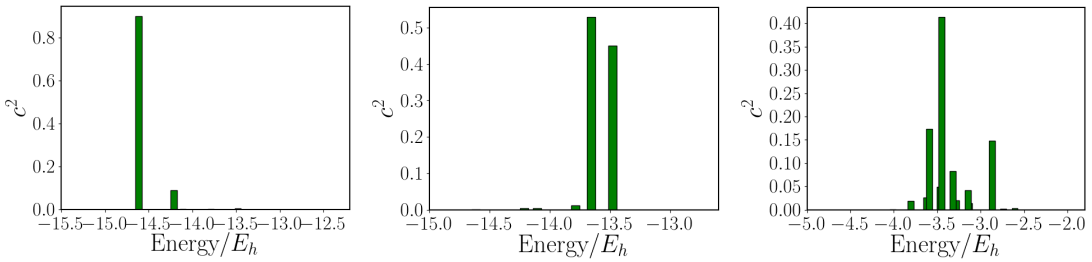

(a) Contributions of the exact states to the ground state reference.

(b) Contributions of the exact states to $1s^23s^2$ reference.

(c) Contributions of the exact states to $2s^23s^2$ reference.

Figure 4.2: Contributions of the exact states of Be in 6-31G basis set to the reference state used in each case.

idea is illustrated in figure 4.2, which shows the contributions (i.e. $|c|^2$) of the exact states, plotted against their energies, to the reference states used in each case. The ground state has only one major contributor with $|c|^2 > 0.8$ so the ground state reference is a good approximation of an exact solution, supporting the observation that the perturbation series for this state converges. On the other hand, the $1s^23s^2$ reference has two almost equal contributions from different exact states and the $2s^23s^2$ reference state is a real multiconfigurational case, showing reasonably high $|c|^2$ from over five exact states. All these states are in the same energy region, confirming that the failure of perturbation theory is at least in part to the many near-degenerate state that exist in the Be atom.[37] Thus, both excited reference states are poor approximations for any single exact state, while the success of perturbation theory lies in the assumption that the exact and unperturbed state are similar and there is a one-to-one mapping between them.

4.1.1 Exceptional points and intruder states

While the perturbation series diverge and therefore the energies given by them are not systematically improvable, they are still useful because they offer information about the position of the exceptional points of the system and the

State	Method	Quadratic		Padé		Intruder state
		EP	$\mid EP \mid$	EP	$\mid EP \mid$	
$1s^2 3s^2$	Δ-SCF	$0.074 \pm 0.261i$	0.271	$0.079 \pm 0.277i$	0.289	$1s^2 3p^2$
	MOM-SCF	$0.289 \pm 0.016i$	0.289	$0.291 \pm 0.012i$	0.292	$1s^2 2p^2$
$2s^2 3s^2$	Δ-SCF	$0.103 \pm 0.044i$	0.112	$0.109 \pm 0.044i$	0.117	$2p^4$
		$-0.126 \pm 0.0206i$	0.128	$-0.139 \pm 0.199i$	0.140	$2s^2 3p^2$
	MOM-SCF	$0.166 \pm 0.024i$	0.168	$0.168 \pm 0.025i$	0.169	$2s^1 2p^2 3s^1$

Table 4.2: Exceptional points in Be 6-31G.

intruder states that cause the divergence.

The exceptional points have been located using both linear and quadratic Padé approximants and varying the order of the polynomials in the approximants. The values that persisted in all cases have been tabulated in table 4.2, as the other ones are just spurious roots of the high-order polynomials used. All the exceptional points lie inside the unit circle, thus explaining the divergence observed in all cases and the magnitude of the EPs agrees with how fast the respective perturbation series diverge: the closer the EP is to the origin, the faster the series diverges. Notably, there is significant disagreement between the EPs position computed using the two methods, confirming that the orbital optimisation does, indeed, change the energy landscape. This change can be both quantitative — changes in the energies of the states — and qualitative — changes in the dominant EPs and the intruder states that are associated with them.

The intruder states causing the EPs in a system can be identified by following a loop in the λ-space around the EP and tracking the reference state. This was achieved by taking small steps in the λ-space, diagonalising the new Hamiltonian and finding the state with the highest overlap to the one in the previous step. Following this procedure, the initial Slater determinant changes into the Slater determinant corresponding to the intruder state. A second loop around the EP recovers the initial reference state. The paths followed in order to find the exceptional points of

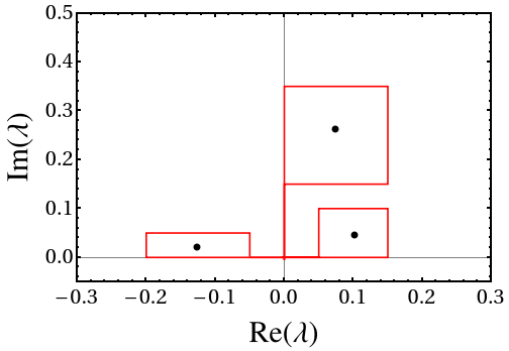

(a) Paths taken to encircle the EPs found using Δ-SCF.

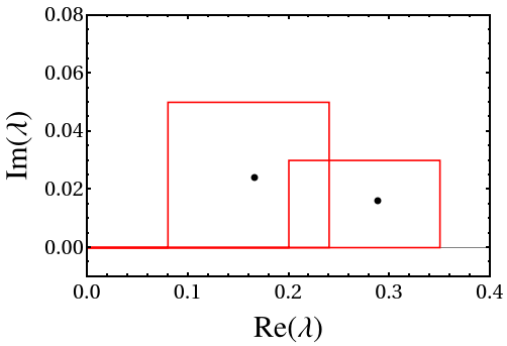

(b) Paths taken to encircle the EPs found using MOM-SCF.

Figure 4.3: Paths taken to encircle the exceptional points for the $1s^2 3s^2$ and $2s^2 3s^2$ states in Be. Each of the paths starts at the origin (which gives the unperturbed reference state), goes in a loop around the exceptional point marked with a black x on the figures and returns at the origin.

the Be system are shown in Figure 4.3. As we expect a rich singularity structure, the patch have to be very tight around the exceptional point to avoid ending up on the wrong state. However, as the positions are just approximations, a larger area in the λ-space needs to be enclosed in the loop, in order to make sure that we do not miss the EP. This method is also a good way of identifying whether a root of the approximant used is an actual EP of the system or just a numerical solution with no physical significance. If it is a true EP, the state will evolve from being similar (high overlap) to the initial state to being similar to the final state. If it is just an unphysical root, this evolution will not be observed.

Figure 4.4 illustrates this for the $2s^2 3s^2$ case using the MOM-SCF method, for which two roots have been found. By encircling the true EP, the reference state gradually evolves from the unperturbed reference state to the intruder state, which is also an eigenstate of the unperturbed Hamiltonian (Figure 4.4a). The root with no physical significance that does not correspond to a true EP does not display this behaviour (Figure 4.4b) and has therefore been omitted from Table 4.2.

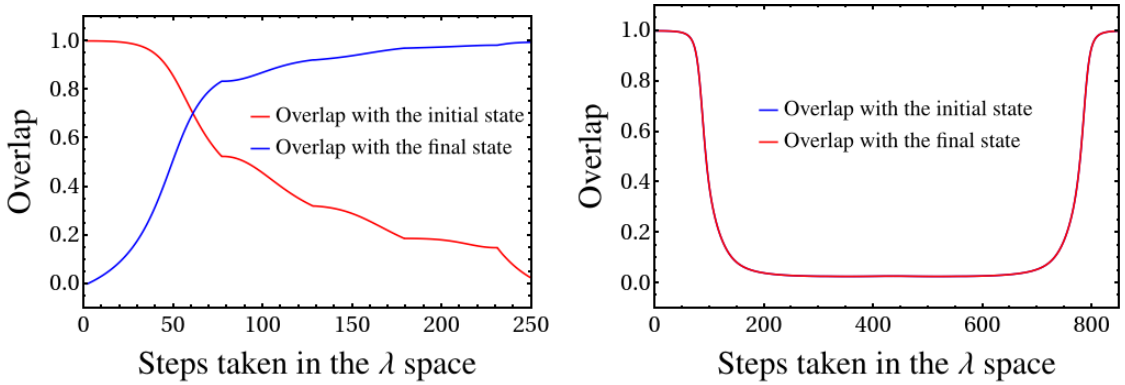

(a) Overlap evolution of the reference state when looping around a true EP of the system.

(b) Overlap evolution of the reference state when looping around a numerical root with no physical significance.

Figure 4.4: Comparison between a true EP and a numerical root with no physical significance. When encircling a true EP, the reference state changes from the initial state to the intruder state, while a numerical root will not show this behaviour.

Table 4.2 lists the intruder states that are causing each of the exceptional points found in the system. There are multiple observations to be made. Firstly, our prediction that the intruder states that cause the dominant EPs are different in the Δ-SCF and MOM-SCF cases. The intruder states in the MOM-SCF calculation are generally lower energy state than those in the Δ-SCF calculation: $1s^2 2p^2$ vs $1s^2 3p^2$, $2s^1 2p^2 3s^1$ vs $2s^2 3p^2$. This means that the MOM-SCF reference states themselves are found at lower energies, which is in agreement with the results obtained for the H_2 molecule: the maximum overlap method brings down the excited state, but this can be at the expense of the shape of the overall landscape and the ordering of the states.

Secondly, the calculations for the $2s^2 3s^2$ excited state found two exceptional points that are influencing the behaviour of the perturbation series. One of them is a front-door intruder and is slightly closer to the origin, while the other one is a back-door intruder. As they are both very close to the origin, none of them is the dominant intruder state. The observation that often MP singularities come in pairs on the negative and positive axis has been previously made and explained

by Sergeev and Goodson.[30]

The two intruder states are the $2s^2 3p^2$ and the $2p^4$ states, which are both found at energies close to the reference state. However, only the $2s^2 3p^2$ state actually couples to the reference state, as the only non-zero non-diagonal matrix terms are those corresponding to double excitations. So this is a case of indirect coupling between the $2s^2 3s^2$ and $2p^4$ states via the $2s^2 3p^2$ which couples with both of them. Therefore, it is not only the states that directly couple with the reference state that can be intruder states and cause divergences in the perturbation series, but any states that can be obtained via a series of double excitations and are found in the appropriate energy region.

Lastly, the intruder state found using the MOM-SCF method for the $2s^2 3s^2$ state is an odd one. While all the other intruder states found have been closed-shell, the $2s^1 2p^2 3s^1$ state is not. It is unclear whether this is a consequence of the MOM or if open-shell states are commonly intruder states for closed-shell references.

4.1.2 Converging the series

While the divergent series are rich in information about the singularity structure of the system, they are unable to give even an estimate of the energy of the state. We will try to overcome this in two different ways and then compare the results.

I. Quadratic approximant

So far in this thesis, the approximants have been used solely for locating the exceptional points of the system. However, their main function is to approximate the value of a series from the first few terms of the series. This approach is very promising for approximating series that diverge because, as seen in equations 2.29 and 2.27, only the first n terms of the MP series are used so the largest terms

in the series are discarded from the calculation.

It was also found that, while the linear approximants are able to determine the position of the EPs with reasonable accuracy, similar to that of the quadratic approximants, the estimates of the energy are very poor, usually too large by several orders of magnitude. This is because the linear approximants model the energy to have the wrong functional form, and approximate the EPs as poles, not square root branch points.

Therefore, we will only be using the estimates computed via the quadratic approximants. As these vary with the order of the polynomials in the approximant, the $[5, 5, 5]$ approximant has been used for all following calculations, as it has been consistently found to give the best approximation to the exact energy.

Notable, the same set of polynomials can describe two different functions for the energy, as seen in equation 2.31. The solution is not consistently the plus or minus solution. However, if a rough estimate of the energy is known (for example, the HF energy of the reference state), the correct solution can be easily chosen.

II. Imaginary level shift

The main reason for the divergence observed in the perturbation series of many systems is the near-degeneracy of states with the reference which causes small denominators in the expressions for the energy corrections in MP theory (see equation 2.15). Thus, even if the matrix element in the numerator is small and the state should not contribute significantly to the total sum, the contribution is actually very large, causing the series to blow up.

A general family of solutions for this problem is that using a level shift.[38, 39, 40, 41] A level shift is, generally, a small number ϵ that is added to the denominator of the

second order correction, in order to avoid divergence due to near-degeneracy:

$$E_n^{(2)} = \sum_{k \neq n} \frac{|\langle \Phi_k^{(0)} | \hat{H}_1 | \Phi_n^{(0)} \rangle|^2}{E_n^{(0)} - E_k^{(0)} - \epsilon} \tag{4.2}$$

As we are working beyond second order, this is actually equivalent to shifting the energies of all the eigenstates of $\hat{H}_0$ by ϵ, with the exception of the reference states. This shift can be included in the general formula 2.17, by replacing $\left(H^{(0)} - E^{(0)}\right)^{-1}$ with $\left(H^{(0)} - E^{(0)} + \epsilon\right)^{-1}$. The level shift makes sure that the determinant of the matrix that is being inverted is large enough. This change translates to equation 4.2 at second order and it can also be applied for higher-order terms.

While this method is found to make the series to converge for a well-chosen ϵ, it is undesirable because it changes the energy of the states in the reference space. However, if ϵ is chosen to be imaginary, the real part of the energy of the unperturbed states is unchanged, while also avoiding small denominators and divergence. The energy corrections can be computed by taking the real part of the result. Therefore, the formulae from Chapter 2 become:

$$\Phi_n^{(k)} = \left(H^{(0)} - E_n^{(0)} + i\epsilon\right)^{-1} \left(\sum_{i=1}^{k} E_n^{(i)} \Phi_n^{(k-1)} - H^{(1)} \Phi_n^{(k-1)}\right) \tag{4.3}$$

$$E_n^{(k)} = Re\left(\langle \Phi_n^{(0)} | \hat{H}_1 | \Phi_n^{(k-1)} \rangle\right) \tag{4.4}$$

Translated into the λ-space we have been using so far, the introduction of the imaginary level shift has the effect of moving the dominant exceptional points. The assumption underlying this method is that the shift is sufficiently small that the energy landscape is not significantly changed and that the most important features are preserved. There have been multiple attempts at developing a method to find the optimal level shift for a system or even to find a set of optimal level shifts so that each state is shifted by a different amount, as using the same level shift for all states might be a bit too simplistic.[40,41] Nevertheless, these methods

usually work by trying to obtain the best possible second-order correction and are not at all concerned with the convergence of the series. In order to ensure the convergence of the series, the level shift needs to move the dominant EP outside the unit circle, whereas if only the second-order correction is concerned, it is sufficient for the shift to move the EP away enough from the origin so that the series diverges slowly and the second-order correction is reasonable in magnitude. For lack of a better alternative, the results in this section have been computed by finding the smallest value of ϵ for which the series converges. While this is feasible with the small systems investigated here, it is desirable to find a better way of identifying the level shift needed to converge the series.

III. Results and discussion

The two different approaches give the results listed in Tables 4.3 and 4.4. By comparing the two results, the quadratic approximant estimates are clearly superior and they are very close to the exact solution. In particular, the solution obtained via the Δ-SCF method for the $1s^2 3s^2$ state is almost exact. For the $2s^2 3s^2$ state, the MOM-SCF method is slightly more accurate, so there is no clear difference in the quality of the two methods. A disadvantage of this method is that it cannot compute the eigenstate corresponding energy so the overlap with the exact solution cannot be investigated. We have also obtained these results using a $[5, 5, 5]$ approximant, which needs 15 terms of the perturbation series to be computed, as they are needed in the equation system that generates the polynomials. This is a lot larger than the one term computed in a simple MP2 calculation.

When we performed the imaginary level shift method, we have chosen the ϵ values that make the series converge in each individual case. Indeed, the exceptional points of the new system have been shifted outside of the unit circle (see Table

State	Method	Energy/E_h	FCI/E_h
$1s^2 3s^2$	Δ-SCF	-13.657916	-13.6579143
	MOM-SCF	-13.660544	-13.6579143
$2s^2 3s^2$	Δ-SCF	-3.414318	-3.449938
	MOM-SCF	-3.341545	-3.449938

Table 4.3: Estimates of Be excited state energies using the $[5, 5, 5]$ quadratic approximant.

State	Method	ϵ	MP2/E_h	Converged energy/E_h	FCI/E_h	Overlap
$1s^2 3s^2$	Δ-SCF	0.2	-13.58872	-13.58241	-13.65791	0.749
	MOM-SCF	0.6	-13.58498	-13.58059	-13.65791	0.741
$2s^2 3s^2$	Δ-SCF	1.3	-3.37459	-3.37579	-3.44993	0.654
	MOM-SCF	1.1	-3.38869	-3.37756	-3.44993	0.657

Table 4.4: Results for Be excited state energies using the imaginary level shift method.

4.5). However, the values of the level shift that converge the series, especially in the case of the $2s^2 3s^2$ state are rather large compared to other values used in literature,[42] making the assumption that the energy landscape of the system does not significantly change upon the level shift seem implausible.

Indeed, the results obtained using the level shift are rather poor, with the MP2 energy being more accurate than the convergent energy. Therefore, the assumption that is crucial for perturbation theory, i.e. that each term in the series takes the energy closer to the exact one, is not correct. The overlap of the converged state with the exact solution is around 0.7 in all cases. There is little dependence on whether the Δ-SCF or the MOM-SCF methods are used. What seems to be more important is the level shift, as the states that need a larger level shift to converge result in solutions with poorer overlap with the exact state. This supports our concern about using level shifts that are so large, comparable even with the energies of the states.

Therefore, while the imaginary level shift method succeeds in making the series converge, accuracy is lost in the process and the quadratic approximant remains the most reliable tool we have found so far. However, none of the methods used have given satisfactory results, leading to the conclusion that Be involves a

State	Method	Quadratic		Pade	
		EP	$\mid EP \mid$	EP	$\mid EP \mid$
$1s^2 3s^2$	Δ-SCF	-1.02 $\pm$ 1.105i	1.504	-1.025 $\pm$ 1.10i	1.503
	MOM-SCF	-0.425$\pm$ 1.206i	1.279	-0.541 $\pm$ 1.138i	1.260
$2s^2 3s^2$	Δ-SCF	0.381 $\pm$ 1.179i	1.240	0.748 $\pm$ 0.955i	1.213
	MOM-SCF	0.95 $\pm$ 1.08i	1.443	0.556 $\pm$ 1.142i	1.271

Table 4.5: Exceptional points in Be excited states after imaginary level shift.

very challenging multiconfigurational character, which cannot be overcome using a simple single-reference method such as the MP theory.

4.2 HF

HF is a diatomic molecule, just like H_2, but because it is a heteroatomic molecule, there is no symmetry being broken upon stretching the bond. In this case, the reference state in which the electrons localise on F is very different in energy to the state in which the electrons localise on H. Therefore, we would expect the perturbation series to be more successful at describing the energies of the excited states in the HF molecule case.

The following results have been obtained by using the STO-3G basis set for the F atom, and the 6-31G basis set for H. The molecular orbital diagram corresponding to this system (excluding the $1s$ orbital on F) is illustrated in Figure 4.5. Of interest to this work are the σ orbitals, which are involved in bonding so we will only consider excited states that involve excitations between σ orbitals. Out of the 10 possible excited states that fall in this category, we are looking specifically at single excitations from the 2σ and 3σ orbitals to the 4σ and 5σ orbitals, respectively. These have been chosen because they couple between each other and with the ground state. Other excited states can be treated in a similar way. If excited states in which the 1π set is not completely filled or empty are investigated, degenerate

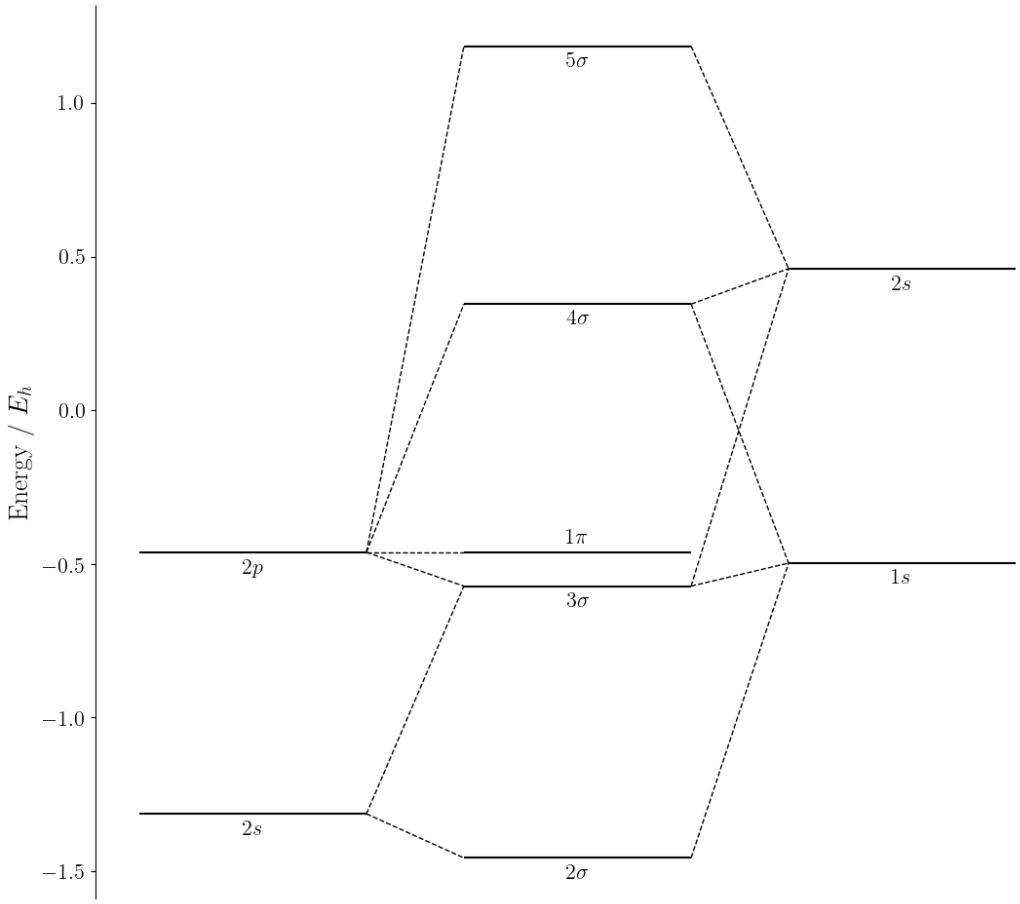

Figure 4.5: Molecular orbital diagram of HF.

perturbation theory must be used.

The energies and positions of exceptional points for the 4 excited states at the equilibrium bond lengths for the ground state are found in Table 4.6. The binding curves for the same excited states are illustrated in Figure 4.6. All the perturbation series diverge and this agrees with the observation that all EPs are inside the unit circle. However, at the MP2 level the divergence is not noticeable and there is little deviation from the HF curve. There is also good agreement between the MP2 energy and the energy computed using the quadratic approximant.

As the H-F bond is stretched, the four excited states show different behaviour. The $3\sigma1\pi4\sigma$ and $2\sigma1\pi5\sigma$ (Fig. 4.6a and 4.6d) perturbation series continue to

State	Method	MP2/E_h	Quadratic/E_h		EP	|EP|
$3\sigma1\pi4\sigma$	Δ-SCF	-95.673	-95.546	-95.694	$0.094 \pm 0.006i$	0.094
	MOM-SCF	-95.501	-93.418	-95.645	$0.033 \pm 0.0007i$	0.033
$3\sigma1\pi5\sigma$	Δ-SCF	-94.006	-93.887	-94.046	$0.150 \pm 0.099i$	0.180
	MOM-SCF	-93.770	-93.137	-93.903	$-0.327 \pm 0.190i$	0.341
$2\sigma1\pi4\sigma$	Δ-SCF	-97.217	-97.454	-94.119	$0.137 \pm 0.081i$	0.160
	MOM-SCF	-97.360	-	-	$-0.683 \pm 0.103i$	0.691
$2\sigma1\pi5\sigma$	Δ-SCF	-95.762	-95.596	-95.773	0.337	0.337
	MOM-SCF	-95.785	-	-	$0.261 \pm 0.015i$	0.262

Table 4.6: Results for HF at the ground state equilibrium geometry. The quadratics used for the energy and the EP localisation are of order [3, 3, 3]. Both solutions of the approximant are given, as they are too close to be told apart by inspection. The values missing in the table are due to the approximant not giving a real value of the energy i.e. the term under the square root in eq. 2.31 is negative.

diverge both wth the MOM-SCF and Δ-SCF reference, but the divergence is not observed at the MP2 level. For these excited states, the binding curves for the MOM-SCF reference are almost identical to those for the Δ-SCF reference, both at the HF and MP2 levels. This indicates that the orbitals in these excited reference states are the same as those in the ground state.

The $2\sigma1\pi4\sigma$ (Fig. 4.6c) state shows a slight discontinuity in the Δ-SCF MP2 binding curve at 1.25Å, after which the divergence is clearer. This resembles similar features also present in the H_2 binding curves in Figures 3.7b and 3.8b, caused by a change in sign in the gradient of the energy landscape at the point of the Taylor expansion. This discontinuity is resolved in the MOM-SCF MP2 binding curve. The MOM-SCF reference still gives a divergent series, but this is not obvious in the MP2 correction. At the HF level, the binding curves are still almost overlapping, so there is little orbital relaxation upon excitation. However, as the divergence of the perturbation series is slowed upon orbital relaxation, we can see that the MP series is sensitive to even the slightest change in the energy of the reference state.

The binding curves for $2\sigma1\pi5\sigma$ (Fig. 4.6b) show some interesting features. At the HF level, there is a clear energy gap between the reference states, with the

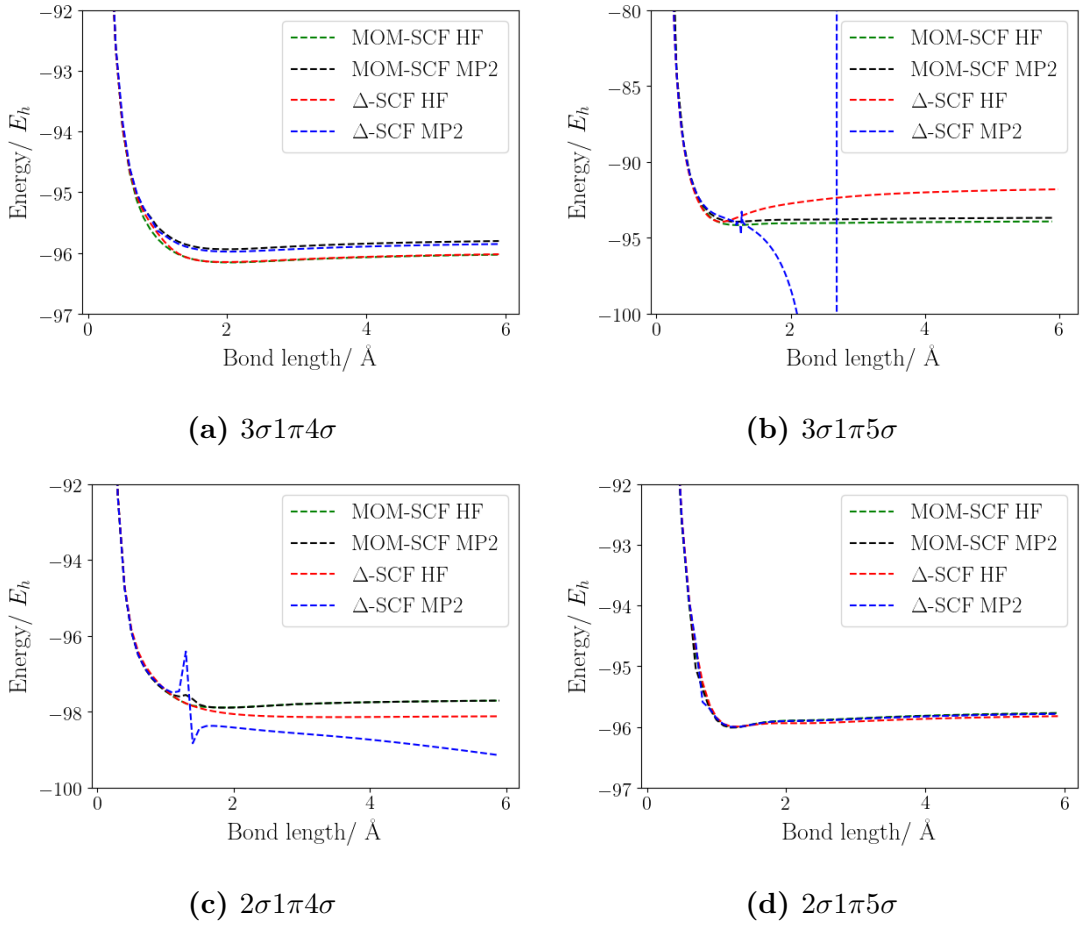

(a) $3\sigma1\pi4\sigma$ **(b)** $3\sigma1\pi5\sigma$

(c) $2\sigma1\pi4\sigma$ **(d)** $2\sigma1\pi5\sigma$

Figure 4.6: Binding curves for 4 excited states of HF as the H-F bond is stretched.

MOM-SCF HF binding curve being significantly lower in energy. This supports our intuition from Chapter 3 that orbital optimisation lowers the energy of excited reference states. At the MP2 level, the Δ-SCF binding curve has a discontinuity at the same bond length as the $2\sigma1\pi4\sigma$ state, implying that these have a common cause. After this discontinuity, the binding curve diverges abruptly. This feature is removed upon orbital optimisation, for which the series diverges more slowly. This indicates that the lowering in the energy of the reference state increases the gap between the targeted state and the states that are near-degenerate to it, creating a less rapidly diverging series.

State	Method	MP2/E_h	Quadratic/E_h		EP	|EP|
$2a_1 1b_2 3a_1 4a_1$	Δ-SCF	-73.888	-73.579	-73.977	0.250 ± 0.093i	0.268
	MOM-SCF	-73.906	-71.943	-74.038	-0.613 ± 0.097i	0.621
$2a_1 1b_2 3a_1 2b_2$	Δ-SCF	-73.687	-73.630	-73.698	0.378 ± 0.573i	0.687
	MOM-SCF	-73.753	-73.651	-74.191	0.627 ± 0.309i	0.699
$2a_1 1b_2 1b_1 4a_1$	Δ-SCF	-73.732	-73.351	-73.746	-0.513±0.309i	0.599
	MOM-SCF	-73.672	-73.596	-75.488	-0.622±0.126i	0.634
$2a_1 1b_2 1b_1 2b_2$	Δ-SCF	-73.740	-73.723	-73.518	-0.087±0.080i	0.118
	MOM-SCF	-75.010	-74.424	-73.512	0.012±0.003i	0.012
$2a_1 3a_1 1b_1 4a_1$	Δ-SCF	-73.229	-73.035	-73.496	-0.088±0.070i	0.113
	MOM-SCF	-73.587	-74.820	-73.433	0.0633±0.005i	0.064
$2a_1 3a_1 1b_1 2b_2$	Δ-SCF	-73.092	-73.075	-73.099	0.632±0.338i	0.717
	MOM-SCF	-73.219	-	-	0.052	0.052
$1b_2 3a_1 1b_1 4a_1$	Δ-SCF	-72.151	-72.074	-72.441	0.0695	0.0695
	MOM-SCF	-72.143	-71.617	-71.822	0.075	0.075
$1b_2 3a_1 1b_1 2b_2$	Δ-SCF	-71.926	-71.841	-72.184	0.297±0.135i	0.326
	MOM-SCF	-72.002	-	-	0.019	0.019

Table 4.7: Results for H_2O at the ground state equilibrium geometry. The quadratics used for the energy and the EP localisation are of order [3, 3, 3]. Both solutions of the approximant are given, as they are too close to be told apart by inspection. The values missing in the table are due to the approximant not giving a real value of the energy i.e. the term under the square root in eq. 2.31 is negative.

4.3 H_2O

Being a polyatomic molecule, H_2O can adopt multiple geometries, as it has more degrees of freedom. For simplicity, we are only going to investigate the excited states of the molecule along the symmetric stretch of the equilibrium geometry. Some other geometries were studied by Warken.[43] The molecular orbital diagram corresponding to this geometry is shown for reference in Figure 4.7. There are 20 possible closed-shell excited states for H_2O in minimal basis set, which is used here, but we will only be looking at those corresponding to double excitations from the $2a_1, 1b_2, 3a_1, 1b_1$ orbitals into the $4a_1, 2b_2$ orbitals i.e. 8 excited states. Similarly to the HF molecule case, they all couple with each other and with the ground state. The calculations and analysis presented here can be easily extended to all the other closed-shell excited states.

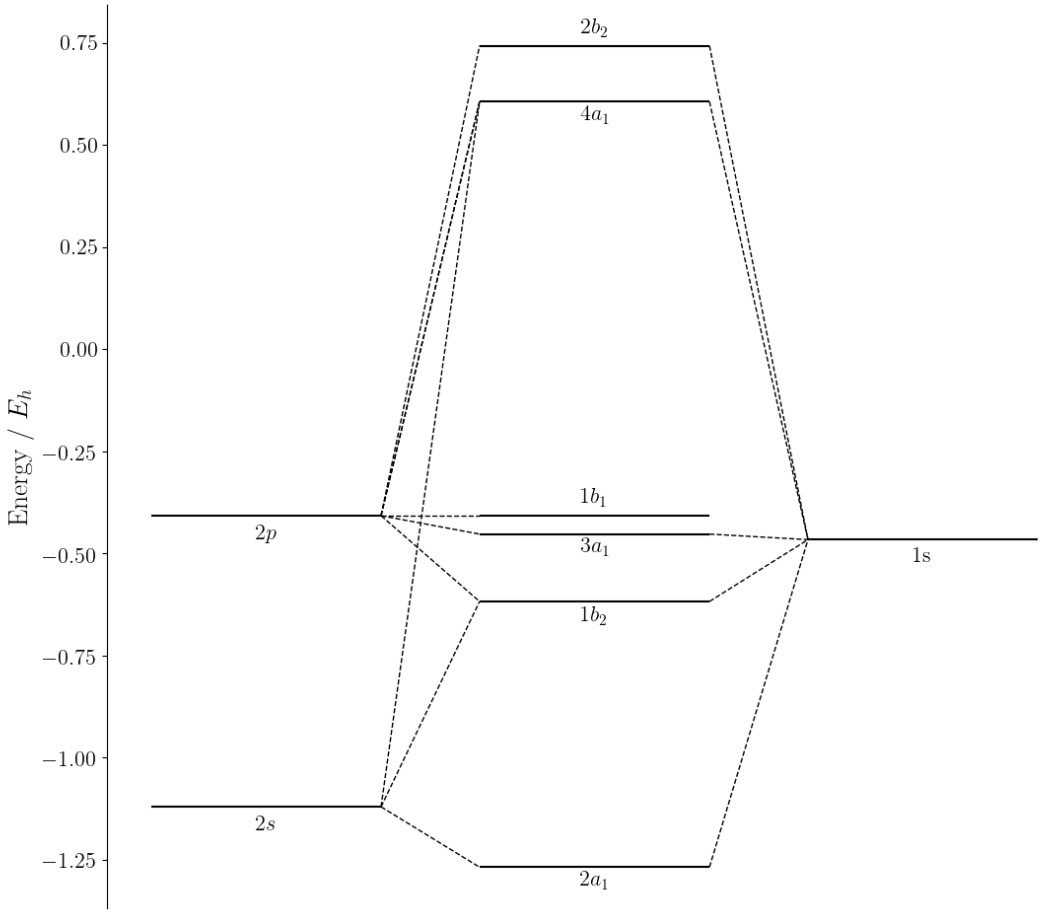

Figure 4.7: Molecular orbital diagram of H_2O.

Table 4.7 lists the results obtained for the eight excited state at the equilibrium geometry of the molecule. It is found that the MP series diverges in all cases, which agrees with all the dominant EPs in the system being inside the unit circle. There are several states for which the exceptional points are found very close to the origin and even directly on the real axis. The Δ-SCF and MOM-SCF methods give comparable results both in MP2 and using the quadratic approximant.

However, on stretching the O-H bond, the two methods show very different results, with the Δ-SCF diverging very rapidly and discontinuously, while the MOM-SCF still diverges, but at a rate that leaves the MP2 values in a reasonable energy range. This is illustrated in Figures 4.8 and 4.9. The only case for which

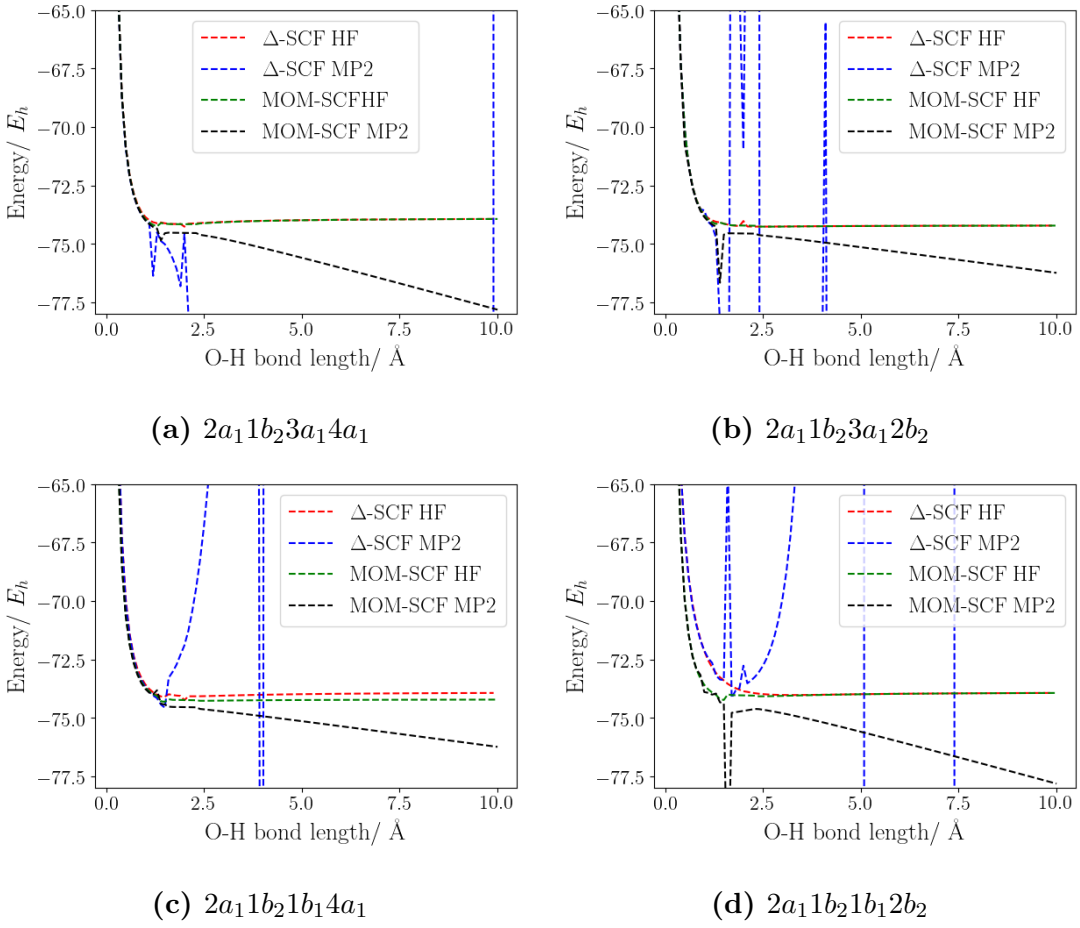

(a) $2a_1 1b_2 3a_1 4a_1$ **(b)** $2a_1 1b_2 3a_1 2b_2$

(c) $2a_1 1b_2 1b_1 4a_1$ **(d)** $2a_1 1b_2 1b_1 2b_2$

Figure 4.8: Binding curves for 4 excited states of H_2O as the O-H bonds are symmetrically stretched.

Δ-SCF MP2 does not show this erratic behaviour is for $1b_2 3a_1 1b_1 2b_2$, which is the highest in energy and reasonably isolated in energy from other states. While it still diverges due to near-degeneracies, the larger energy gaps ensure that at the MP2 level, this divergence is not observed.

The plots in Figures 4.8 and 4.9 elucidate another property of the MOM optimisation that has already been mentioned for previous system: the effect of the optimisation is that of lowering the energy of the targeted reference state, or leaving it practically unchanged, as observed for the HF molecule calculations. The first seven targeted excited states are all close in energy and near-degenerate in the Δ-SCF calculation, which makes use of the reference energy landscape of the ground

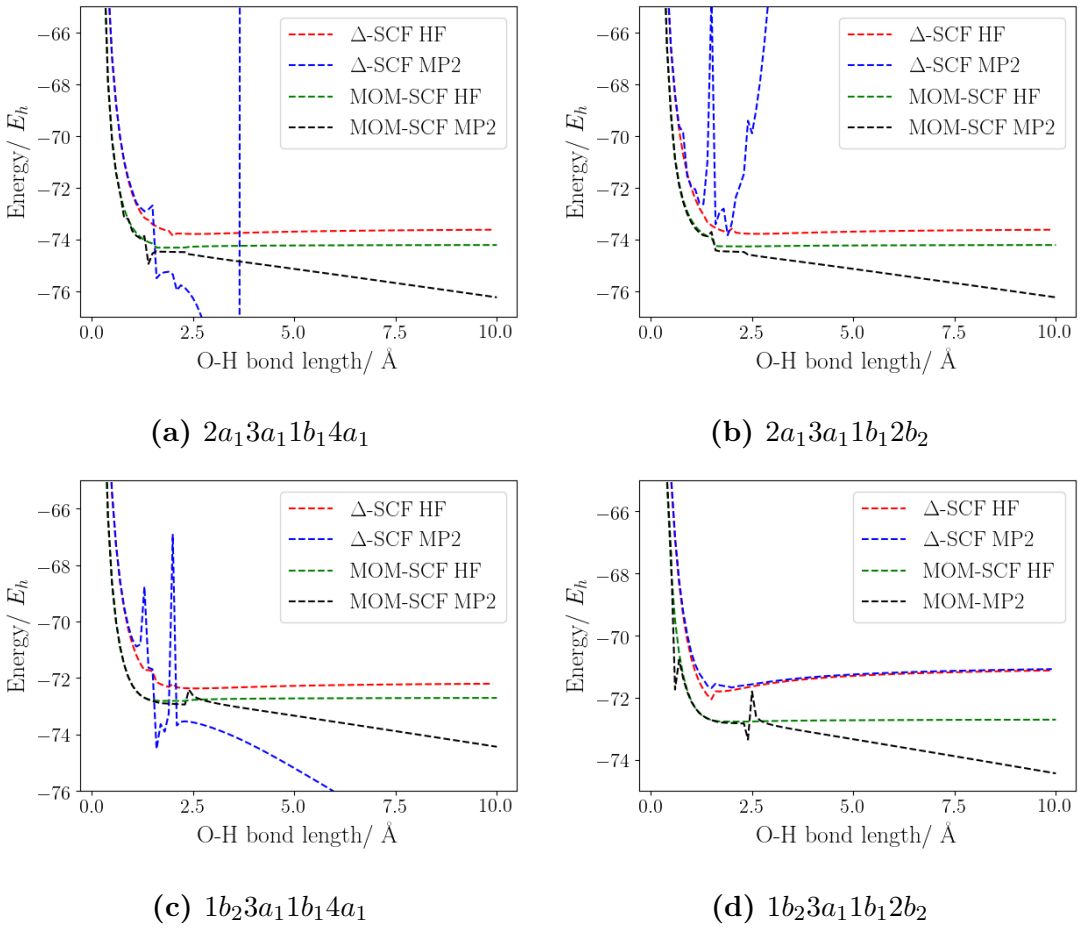

(a) $2a_1 3a_1 1b_1 4a_1$ **(b)** $2a_1 3a_1 1b_1 2b_2$

(c) $1b_2 3a_1 1b_1 4a_1$ **(d)** $1b_2 3a_1 1b_1 2b_2$

Figure 4.9: Binding curves for 4 excited states of H_2O as the O-H bonds are symmetrically stretched.

state. Upon orbital relaxation, the reference state corresponding to the excited state of interest is lowered in energy and the energy gaps are increased. This leads to an improved MP2 series. On the other hand, the eighth excited state is already in an area of low density of states. When it is lowered by the optimisation procedure, the gap with the other states is decreased and the perturbation series diverges faster.

Therefore, the MOM-SCF method is not inherently more or less accurate than the Δ-SCF method, as its success depends on the energy spectrum of the system and on the position of the targeted state on that spectrum.

4.4 Discussion

The results from this chapter consistently show that the MP series diverges for the excited states of simple molecules and small atoms, independent of which of the two sets of reference states are used. Nevertheless, at the MP2 level we see a range of results.

In general, the use of Δ-SCF reference states is either giving a good MP2 energy, or a series with very rapid divergence. The use of the MOM-SCF references improves the convergences if the Δ-SCF method is clearly diverging, but makes the series diverge faster if the Δ-SCF method is giving good MP2 energies. Thus, this confirms that orbital optimisation does affect the energy of the reference, but not necessarily in a way that favours a perturbative approach. The effect depends on whether the lowering of the reference energy resulted from orbital optimisation increases or decreases the energy gap between the targeted states and the nearby states in the energy spectrum. Whether this is the case or not can be decided using chemical intuition for small systems, but becomes impossible for bigger molecules.

The energies obtained for the HF molecule at the MP2 level are generally good, especially when using the MOM-SCF excited reference states, whereas those for H_2O are poor with both methods. Previous studies show that MP theory can fail for H_2O even in the ground states, depending on the basis set being used.[17] This shows there is significant dependence on the chemical system. In particular, the orbitals of the HF molecule (Fig. 4.5) are more spaced out than those in H_2O (Fig. 4.7), so states with different orbital occupation do not have similar energies. On the other hand, H_2O has two sets of orbitals that are near-degenerate, namely the $3a_1$ and $1b_1$ orbitals, as well as the $4a_1$ and $2b_2$ orbitals. Upon orbital optimisation, the orbitals of HF do not change significantly in energy in any of the

excited states considered, whereas for H_2O, the orbitals are very different from one excited state to another and have multiple near-degeneracies and reorderings of the orbital energies. The MO diagrams for two non-equilibrium geometries of the two molecules are included in Appendix B and confirm that the general effect of the MOM algorithm is to lower the energies of the occupied orbitals. Therefore, a good intuition for predicting the performance of MP theory for a system is given by the molecular orbital spacings in the molecule. However, this limits the applicability of a perturbative approach to a small set of excited states in molecules of reduced dimensions, as bigger molecules have more MOs with even smaller spacing.

We lack the energies calculated for the excited states considered here using different methods, as well as the FCI energies due to the fact that it is difficult to assign an exact state to each reference excited state. Therefore, we cannot assess the accuracy of the MP2 values. However, for the majority of cases there is abrupt divergence even at the MP2 level. This is observed more clearly for the Δ-SCF references than for the MOM-SCF ones, but the data collected is not favourable for either of the two methods.

5
Conclusions

Møller–Plesset perturbation theory was used for the excited states of a series of molecular and atomic systems. Two different sets of excited reference states were used, one which used the same orbitals as in the ground state of the molecule (Δ-SCF) and one that used the optimal orbitals for each excited state (MOM-SCF). By allowing the perturbation parameter λ to take values in the complex plane, the singularity structure of the energy in the λ-space was investigated. Linear and quadratic approximants were used to locate the exceptional points of $E(\lambda)$, which are indicators of whether the perturbation series converges or diverges, as the convergence of the perturbation series is essential for the method to be systematically improvable.

It was found that the perturbation series diverges for all excited states of the systems considered at all geometries, with the exception of the H_2 molecule. The imaginary level shift method was used to achieve the convergence of the series, but the values of the level shifts needed were found big, comparable to the energy of the targeted states, leading the series to converge to the wrong energy. The extrapolation of the energy by using quadratic approximants was found to give the most accurate

results, but this method provides no information on the final wave function so any other properties of the system such as spin or electric dipole cannot be computed.

Excited state perturbation theory proved to be challenging due to near-degeneracies and high density of states in the chemical systems investigated. Considering the poor performance of MP theory even in small systems, it is not expected for it to perform well in larger molecules in this form. While the list of choices of the reference used in this thesis is not exhaustive, we can generally say that a single-reference perturbative approach is bound to diverge for all but very specific cases.

Therefore, further research into excited states should focus on finding and optimising multi-references approaches, which have the drawback of being computationally expensive. The most natural choice is that of constructing the reference as a linear combination of Slater determinants, as is done in configuration interaction (CI). The Slater determinants being used could be specific eigenvectors of the Δ-SCF reference, in which case they would be orthogonal, but a different approach could use states that have been individually optimised, giving a non-orthogonal configuration interaction approach (NOCI).[44] Coupled-cluster theory has also been used to treat excited states,[45,46] but the most commonly used method remains CASPT2.[47]

Bibliography

1. González, L.; Escudero, D.; Serrano-Andrés, L. *ChemPhysChem* **2012**, *13*, 28–51.
2. Atkins, P. W.; Friedman, R. *Molecular Quantum Mechanics*; Oxford University Press, 2010.
3. Helgaker, T.; Jorgensen, P.; Olsen, J. *Molecular Electronic-Structure Theory*; John Wiley & Sons, 2014.
4. Gilbert, A. T. B.; Besley, N. A.; Gill, P. M. W. *J. Phys. Chem. A* **2008**, *112*, 13164–13171.
5. Besley, N. A.; Gilbert, A.; Gill, P. M. *J. Phys. Chem.* **2009**, *130*, 124308.
6. Barca, G. M.; Gilbert, A.; Gill, P. M. *J. Phys. Chem.* **2014**, *141*, 111104.
7. Møller, C.; Plesset, M. S. *Phys. Rev.* **1934**, *46*, 618–622.
8. Bartlett, R. J. *Annu. Rev. Phys. Chem.* **1981**, *32*, 359–401.
9. Bartlett, R. J.; Musiał, M. *Rev. Mod. Phys.* **2007**, *79*, 291–352.
10. Cremer, D. *Wiley Interdiscip. Rev. Comput. Mol. Sci.* **2011**, *1*, 509–530.
11. Szabo, A.; N.S., O. *Modern Quantum Chemistry*; Dover Publications Inc., 1989.
12. Born, M.; Oppenheimer, J. *Ann. Phys.* **1927**, *389*, 457.
13. Purwanto, W.; Al-Saidi, W.; Krakauer, H. *J. Chem. Phys.* **2008**, *128*, 114309.
14. Mori-Sánchez, P.; Cohen, A. J. *J. Chem. Phys.* **2014**, *140*, 044110.
15. Rayleigh, J. *The Theory of Sound* **1894**, 115–118.
16. Schrödinger, E. *Ann. Phys.* **1926**, *385*, 437 – 490.
17. Olsen, J.; Christiansen, O.; Koch, H.; Jo/rgensen, P. *J. Chem. Phys.* **1996**, *105*, 5082–5090.
18. Olsen, J.; Jørgensen, P.; Helgaker, T.; Christiansen, O. *J. Chem. Phys.* **2000**, *112*, 9736–9748.
19. Laidig, W. D.; Fitzgerald, G.; Bartlett, R. J. *Chem. Phys. Lett.* **1985**, *113*, 151–158.
20. Leininger, M. L.; Allen, W. D.; Sherrill, D. *J. Chem. Phys.* **2000**, *112*, 9213–9222.
21. Bender, C. M.; Orszag, S. A. *Advanced Mathematical Methods for Scientists and Engineers I: Asymptotic Methods and Perturbation Theory*; Springer New York, 1999.

22. Goodson, D. *Wiley Interdiscip. Rev.-Comput. Mol. Sci.* **2000**, *2*, 743–761.

23. Tinker, M.; Lambourne, R. *Further Mathematics for the Physical Sciences*; John Wiley & Sons, 2000.

24. Marie, A.; Burton, H. G. A.; Loos, P.-F. *J. Phys.: Condens. Matter* **2021**, *33*, 283001.

25. Benda, Z.; Jagau, T.-C. *J. Phys. Chem. Lett.* **2018**, *9*, 6978–6984.

26. Bender, C. M.; Dorey, P.; Dunning, T. C.; A., F. *PT Symmetry in Quantum and Classical Physics*; Singapore: World Scientific, 2019.

27. Farkas, H. M.; Kra, I. *Riemann Surfaces*; Springer New York, 1992.

28. Durand, P.; Malrieu, J. *Adv. Chem. Phys.* **1987**, *117*, 321.

29. Christiansen, O.; Olsen, J.; Jørgensen, P.; Koch, H.; Malmqvist, P.-A. *Chem. Phys. Lett.* **1996**, *261*, 369–378.

30. Sergeev, A. V.; Goodson, D. Z. *J. Chem. Phys.* **2006**, *124*, 094111.

31. Sergeev, A. V.; Goodson, D. Z.; Wheeler, S. E.; Allen, W. D. *J. Chem. Phys.* **2005**, *123*, 064105.

32. Stillinger, F. H. *J. Phys. Chem.* **2000**, *112*, 9711–9715.

33. Burton, H. G. A.; Thom, A. J. W.; Loos, P.-F. *J. Chem. Phys.* **2019**, *150*, 041103.

34. Fasondini, M.; Hale, N.; Spoerer, R.; Weideman, J. *Comput. Res. Model.* **2019**, *11*, 1017–1031.

35. Burton, H. G. A.; Wales, D. J. *J. Chem. Theory Comput.* **2021**, *17*, 151–169.

36. Goodson, D. Z.; Sergeev, A. V. *Advances in Quantum Chemistry* **2004**, *47*, 193–208.

37. Ivanov, M.; Schmelcher, P. *Eur. Phys. J. D* **2001**, *14*, 279–288.

38. Roos, B. O.; Andersson, K. *Chem. Phys. Lett.* **1995**, *245*, 215–223.

39. Forsberg, N.; Malmqvist, P.-. *Chem. Phys. Lett.* **1997**, *274*, 196–204.

40. Szabados, A.; Surján, P. *Chem. Phys. Lett.* **1999**, *308*, 303–309.

41. Surján, P.; Rolik, Z.; Szabados, A.; Köhalmi, D. *Ann. Phys.* **2004**, *13*, 223–231.

42. Stück, D.; Head-Gordon, M. *J. Chem. Phys.* **2013**, *139*, 244109.

43. Warken, M. *J. Chem. Phys.* **1995**, *103*, 5554–5564.

44. Burton, H.; Thom, A. *J. Chem. Theory Comput.* **2020**, *16*, 5586–5600.

45. Marie, A.; Kossoski, F.; Loos, P-F. *J. Chem. Phys.* **2021**, *155*, 104105.

46. Kossoski, F.; Marie, A.; Scemama, A. et al. *J. Chem. Theory Comput.* **2021**, *17*, 4756–4768.

47. Andersson, K.; Malmqvist, P.; Roos, B. et al. *J. Phys. Chem.* **1990**, *94*, 5483–5488.

Appendices

A

The Slater-Condon rules

The Slater-Condon rules are a set of expressions that can be used to construct the matrix representation of an operator.

In the following, we are going to use Ψ to refer to an arbitrary Slater determinant, Ψ_i^a to refer to a single-replacement Slater determinant, in which an electron from the orbital i has been excited into the orbital a, and Ψ_{ij}^{ab} to refer to a double-replacement Slater determinant, in which an electron from orbital i and an electron from orbital j have been excited to orbitals a and b, respectively.

The full Hamiltonian of a molecule can be expressed in term of a constant term, and one-electron and two-electron operators:

$$\hat{H} = C + \sum_i h(i) + \sum_i \sum_{j<i} \frac{1}{r_{ij}} \tag{A.1}$$

where C is the potential energy of the fixed nuclei interacting with each other, $h(i)$ is the one-body electron operator giving the interaction between electrons and the fixed nuclei, and $\frac{1}{r_{ij}}$ is the two-electron part, giving the interelectronic interaction. The matrix elements of each of these parts of the full Hamiltonian are as follows:

1. C

$$\langle \Psi | C | \Psi \rangle = C \tag{A.2}$$

$$\langle \Phi | C | \Psi \rangle = 0, \Phi \neq \Psi \tag{A.3}$$

2. $h(i)$

$$\langle \Psi | \sum_i h(i) | \Psi \rangle = \sum_i h_{ii} \tag{A.4}$$

$$\langle \Psi_i^a | \sum_i h(i) | \Psi \rangle = h_{ai} \tag{A.5}$$

$$\langle \Phi | \sum_i h(i) | \Psi \rangle = 0, \Phi \neq \{\Psi, \Psi_i^a\} \tag{A.6}$$

3. $\frac{1}{r_{ij}}$

$$\langle \Psi | \sum_i \sum_{j<i} \frac{1}{r_{ij}} | \Psi \rangle = \sum_i \sum_{j<i} [\langle ii|jj\rangle - \langle ij|ij\rangle] \tag{A.7}$$

$$\langle \Psi_i^a | \sum_i \sum_{j<i} \frac{1}{r_{ij}} | \Psi \rangle = \sum_j [\langle ai|jj\rangle - \langle aj|ij\rangle] \tag{A.8}$$

$$\langle \Psi_{ij}^{ab} | \sum_i \sum_{j<i} \frac{1}{r_{ij}} | \Psi \rangle = \langle ai|bj\rangle - \langle aj|bi\rangle \tag{A.9}$$

$$\langle \Phi | \sum_i \sum_{j<i} \frac{1}{r_{ij}} | \Psi \rangle = 0, \Phi \neq \{\Psi, \Psi_i^a, \Psi_{ij}^{ab}\} \tag{A.10}$$

Thus, the summed matrix elements are:

$$\langle \Psi | \hat{H} | \Psi \rangle = \sum_i h_{ii} + \sum_i \sum_{j<i} [\langle ii|jj\rangle - \langle ij|ij\rangle] \tag{A.11}$$

$$\langle \Psi_i^a | \hat{H} | \Psi \rangle = h_{ai} + \sum_j [\langle ai|jj\rangle - \langle aj|ij\rangle] \tag{A.12}$$

$$\langle \Psi_{ij}^{ab} | \hat{H} | \Psi \rangle = \langle ai|bj\rangle - \langle aj|bi\rangle \tag{A.13}$$

All the other matrix elements are 0.

B

The Effect of Orbital Optimisation

The effect of orbital optimisation is investigated for HF and H_2O at two different geometries, at which at least some of the excited states MP series show a clear difference between the Δ-SCF reference and the MOM-SCF reference. This is done by inspecting the MO diagrams of these systems when MOM is applied targeting different excited states.

B.1 HF

Figure B.1 shows the MO diagram for the ground state of HF at 1.8Å and figures B.2 – B.5 show the MO diagrams for 4 excited states of HF after MOM is applied. The general observation is that when an orbital that is not filled in the ground state is occupied in the excited state, its energy is lowered, thus explaining the consistency of our results in which the MOM lowers the energy of the excited states. Orbitals that are occupied in the ground state and unoccupied in the excited state have higher energy. However, the energy changes are small enough so that the ordering of the orbitals is not affected in any of the states and there are no near-degeneracies between σ orbitals, which are the ones involved in the excitations considered.

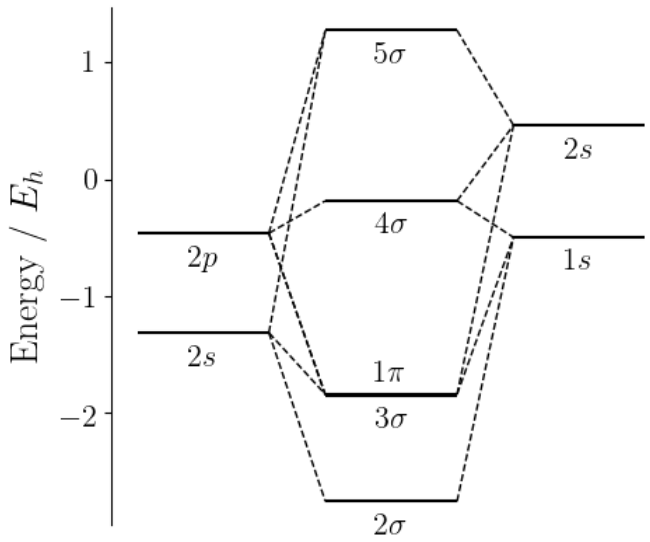

Figure B.1: Δ-SCF orbital energies for HF at 1.8 Å bond length.

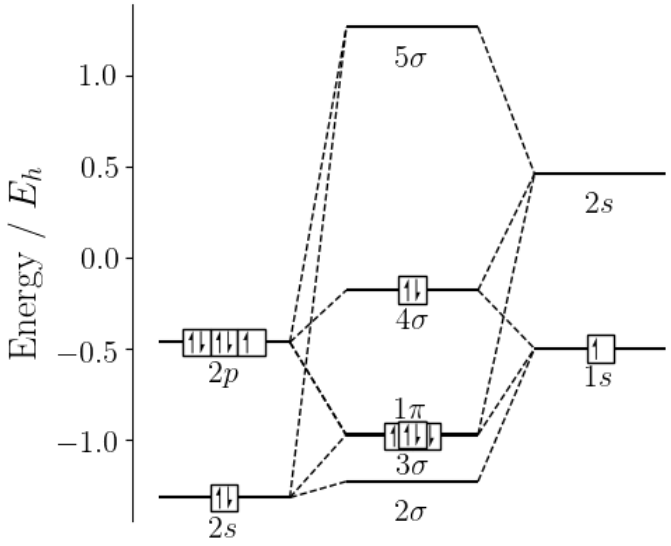

Figure B.2: Optimised MO diagram for the $3\sigma 1\pi 4\sigma$ state of HF at 1.8 Å bond length.

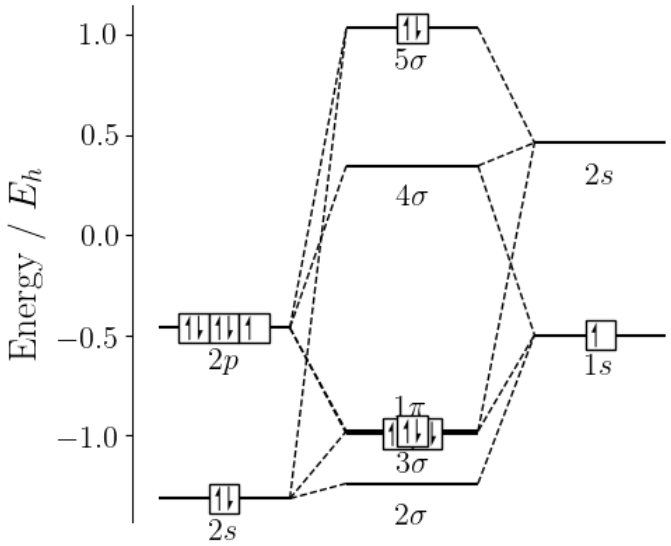

Figure B.3: Optimised MO diagram for the $3\sigma 1\pi 5\sigma$ state of HF at 1.8 Å bond length.

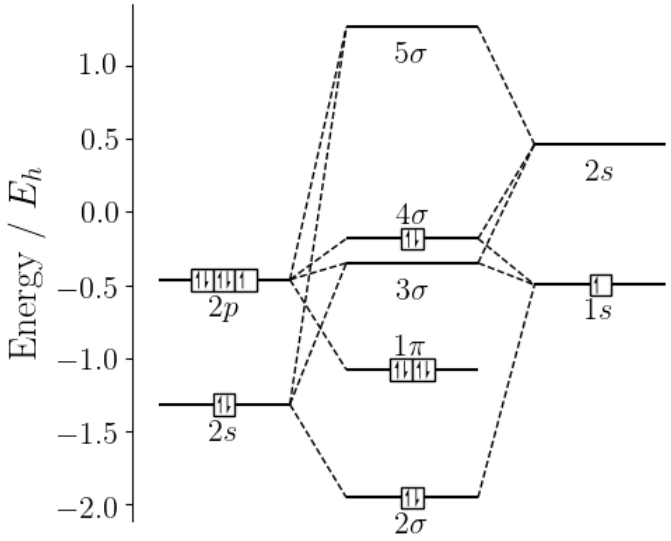

Figure B.4: Optimised MO diagram for the $2\sigma 1\pi 4\sigma$ state of HF at 1.8 Å bond length.

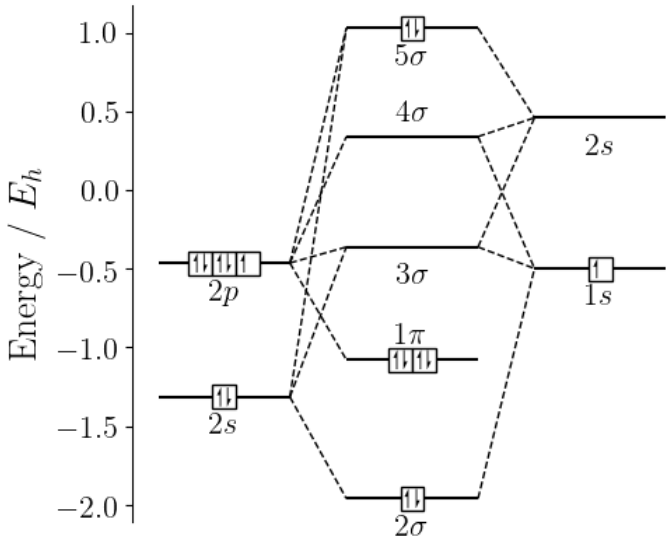

Figure B.5: Optimised MO diagram for the $2\sigma 1\pi 5\sigma$ state of HF at 1.8 Å bond length.

B.2 H_2O

Figure B.6 shows the MO diagram for the ground state of H_2O when the O-H bond lengths are 3.0 Å and figures B.7 – B.14 show the MO diagrams for 8 excited states of H_2O after MOM is applied. The change in the orbital energies after using MOM is tremendous for some of the excited states, with a lot of orbitals becoming near-degenerate. Because of this, it was difficult to identify the orbitals in the optimised MO diagrams, so orbital labels have been omitted from these figures. The considerable effect of orbital optimisation explains why there is a big difference between the results obtained using the two different references in the case of H_2O and a much less significant difference for HF.

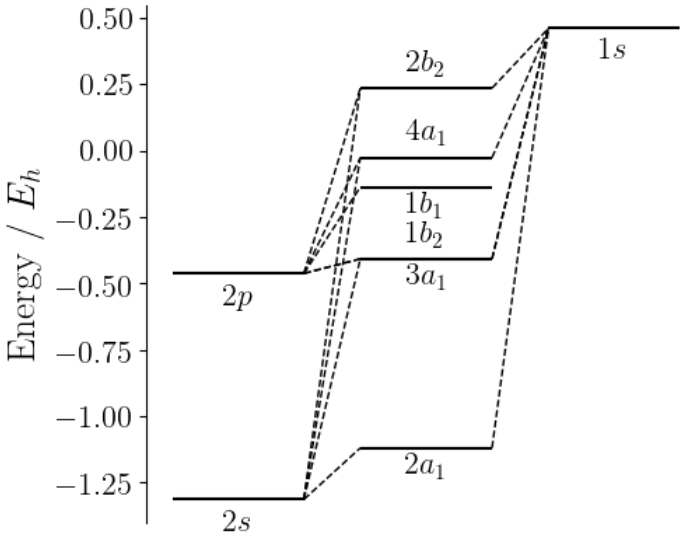

Figure B.6: Δ-SCF orbital energies for H_2O at 3.0 Å O-H bond length.

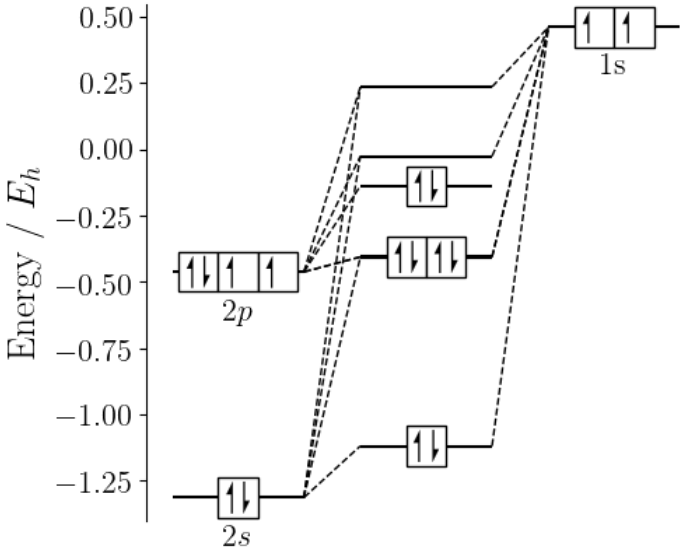

Figure B.7: Optimised MO diagram for the $2a_1 1b_2 3a_1 4a_1$ state of H_2O at 3.0 Å O-H bond length.

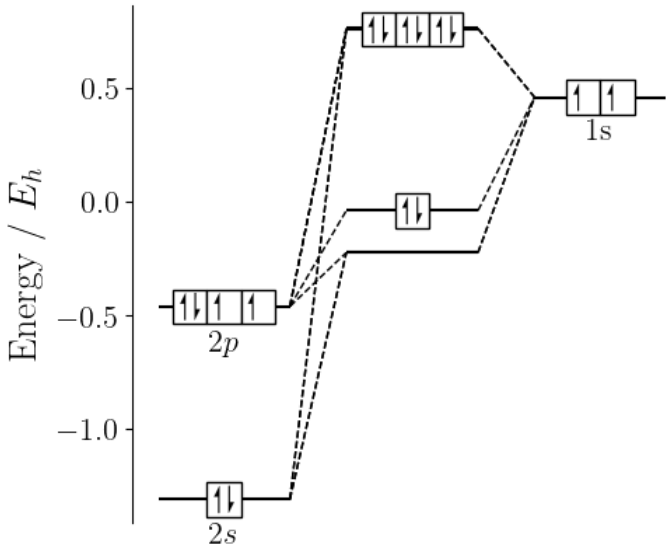

Figure B.8: Optimised MO diagram for the $2a_1 1b_2 3a_1 2b_2$ state of H_2O at 3.0 Å O-H bond length.

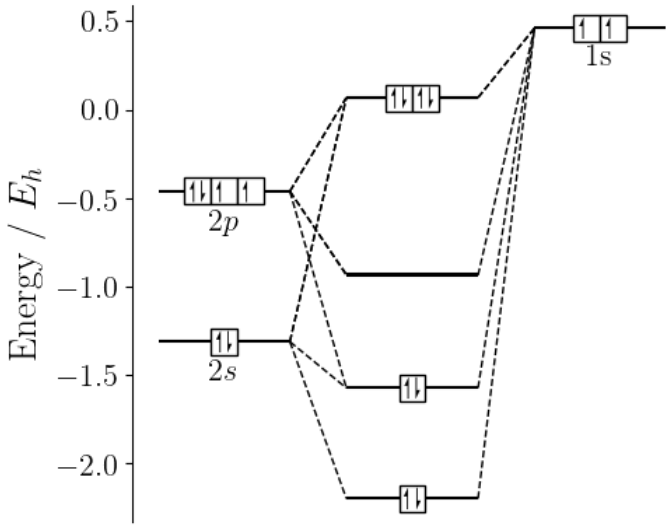

Figure B.9: Optimised MO diagram for the $2a_1 1b_2 1b_1 4a_1$ state of H_2O at 3.0 Å O-H bond length.

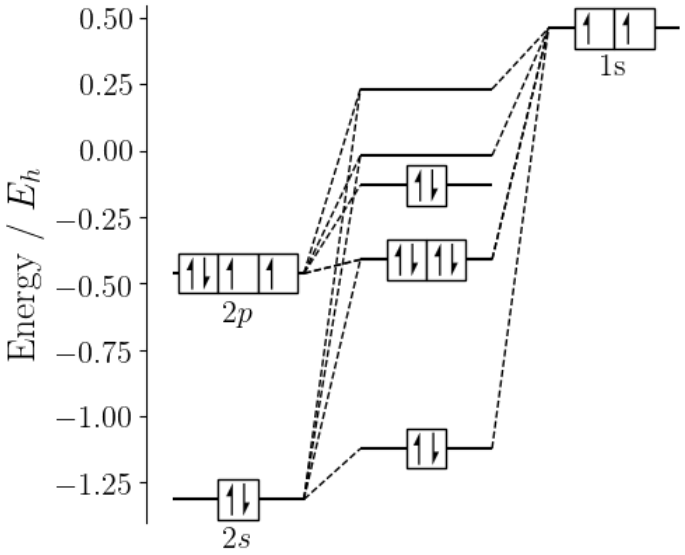

Figure B.10: Optimised MO diagram for the $2a_1 1b_2 1b_1 2b_2$ state of H_2O at 3.0 Å O-H bond length.

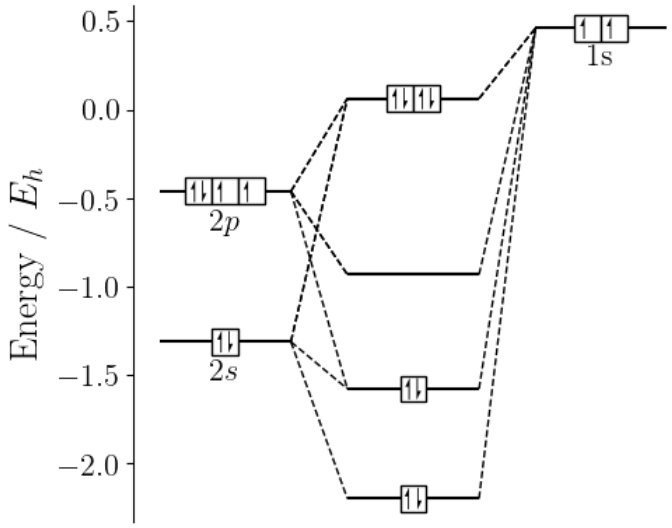

Figure B.11: Optimised MO diagram for the $2a_1 3a_1 1b_1 4a_1$ state of H_2O at 3.0 Å O-H bond length.

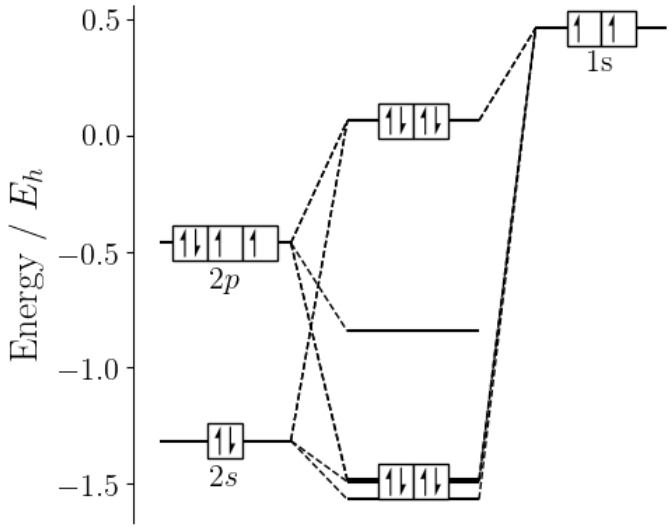

Figure B.12: Optimised MO diagram for the $2a_1 3a_1 1b_1 2b_2$ state of H_2O at 3.0 Å O-H bond length.

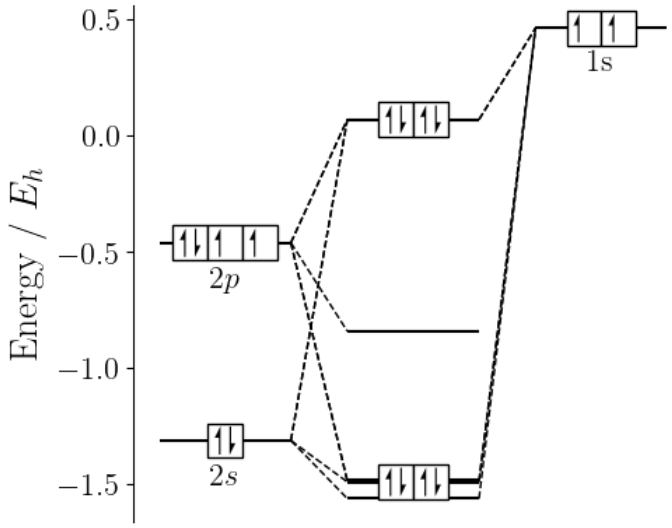

Figure B.13: Optimised MO diagram for the $1b_2 3a_1 1b_1 4a_1$ state of H_2O at 3.0 Å O-H bond length.

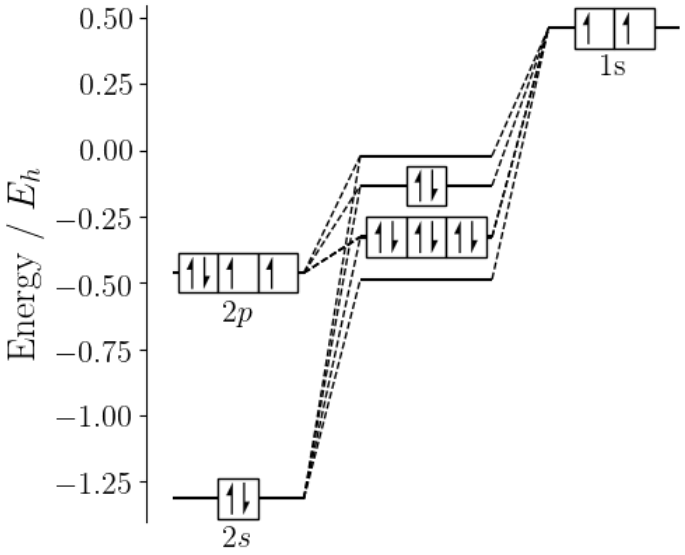

Figure B.14: Optimised MO diagram for the $1b_2 3a_1 1b_1 2b_2$ state of H_2O at 3.0 Å O-H bond length.